Chapter 2

Probing the Interiors of Very Hot Jupiters Using Transit Light Curves

This chapter will be published in its entirety under the same title by authors D. Ragozzine and A. S. Wolf in the *Astrophysical Journal*, 2009. Reproduced by permission of the American Astronomical Society.

Abstract

Accurately understanding the interior structure of extra-solar planets is critical for inferring their formation and evolution. The internal density distribution of a planet has a direct effect on the star-planet orbit through the gravitational quadrupole field created by the rotational and tidal bulges. These quadrupoles induce apsidal precession that is proportional to the planetary Love number (k_{2p}, twice the apsidal motion constant), a bulk physical characteristic of the planet that depends on the internal density distribution, including the presence or absence of a massive solid core. We find that the quadrupole of the planetary tidal bulge is the dominant source of apsidal precession for very hot Jupiters ($a \lesssim 0.025$ AU), exceeding the effects of general relativity and the stellar quadrupole by more than an order of magnitude. For the shortest-period planets, the planetary interior induces precession of a few degrees per year. By investigating the full photometric signal of apsidal precession, we find that changes in transit shapes are much more important than transit timing variations. With its long baseline of ultra-precise photometry, the space-based *Kepler* mission can realistically detect apsidal precession with the accuracy necessary to infer the presence or absence of a massive core in very hot Jupiters with orbital eccentricities as low as $e \simeq 0.003$. The signal due to k_{2p} creates unique transit light curve variations that are generally not degenerate with other parameters or phenomena. We discuss the plausibility of measuring k_{2p} in an effort to directly constrain the interior properties of extra-solar planets.

2.1 Introduction

Whether studying planets within our solar system or planets orbiting other stars, understanding planetary interiors represents our best strategy for determining their bulk composition, internal dynamics, and formation histories. For our closest neighbors, we have had the luxury of sending spacecraft to accurately measure the higher-order gravity fields of these objects, yielding invaluable constraints on their interior density distributions. Using these observations, we have been able, for instance, to infer the presence of large cores, providing support for the core-accretion theory of planet formation (Guillot, 2005). Study of planets outside our solar system, however, has necessitated the development and usage of more indirect techniques. Nevertheless, as the number of well-characterized extra-solar planets grows, we gain more clues that help us answer the most fundamental questions about how planets form and evolve.

Guided by our current understanding of planetary physics, we have begun to study the interiors of extra-solar planets. This endeavor has been dominated by a model-based approach, in which the mass and radius of a planet are measured using radial velocity and transit photometry observations, and the interior properties are inferred by finding the model most consistent with those two observations. This strategy clearly requires a set of assumptions, not the least of which is that the physical processes at work in extra-solar planets are just like those that we understand for our own giant planets. While it does seem that this approach is adequate for explaining most of the known transiting planets, there does exist a group of planets for which the usual set of assumptions are not capable of reproducing the observations (e.g., Guillot et al., 2006; Burrows et al., 2007). These are the planets with so-called positive "radius anomalies", including the first-discovered transiting planet HD 209458b (Charbonneau et al., 2000). Though most of these planets can be explained by adjusting different pieces of the interior physics in the models (including opacities, equations of state, and heat deposition), it is currently impossible to discern which combination of these possible explanations is actually responsible for their observed sizes (Guillot et al., 2006).

Additional uncertainties also exist for planets at the other end of the size spectrum. For the group of under-sized extra-solar planets, such as HD 149026b, the canonical approach is to give the planet a massive highly condensed core of heavy elements in order to match the observed radius. This approach also provides a first order estimate of the planet's bulk composition, in terms of its fraction of heavy elements. There is also the added complication of how the assumed state of differentiation affects the inferred composition and predicted structure (Baraffe et al., 2008).

Currently, the most promising approach to modeling the distinctive features of extra-solar planet interiors is to study the known transiting planets as an ensemble. The group can be used to develop either a single consistent model that reproduces all the observations (e.g., Guillot et al., 2006) or to showcase the possible diversity in model parameters (e.g., opacities, as in Burrows et al., 2007).

Surely, a model-independent measure of interior structure would be valuable in order to begin disentangling otherwise unconstrained physics.

The idea of obtaining direct structural measurements for distant objects is by no means a new one. For decades, the interiors of eclipsing binary stars have been measured by observing "apsidal motion," i.e., precession of the orbit due to the non-point-mass component of the gravitational field (Russell, 1928; Cowling, 1938; Sterne, 1939a,b). The signal of the changing orbit is encoded in the light curves of these systems by altering the timing of the primary and secondary eclipses. From these eclipse times, it is straightforward to determine the so-called apsidal motion constant which then constrains the allowed interior density distributions. Interior measurements inferred from apsidal precession were among the first indications that stars were highly centrally condensed. While it seems non-intuitive, we show in this paper that we can use a similar technique to measure the interior properties of very hot Jupiters. Most surprisingly, the interior structure signal for very hot Jupiters actually dominates over the signal from the star, yielding an unambiguous determination of planetary interior properties.

Our theoretical analysis is also extended to full simulated photometry in order to explore the observability of apsidal precession. We show that this precession is observable by measuring the subtle variations in transit light curves. The photometric analysis is focused on the data expected from NASA's *Kepler* mission, which successfully launched on March 6, 2009 (Borucki et al., 2003; Koch et al., 2006). *Kepler* will obtain exquisite photometry on $\sim$100,000 stars, of which about 30 are expected to host hot Jupiters with periods less than 3 days (Beatty & Gaudi, 2008). *Kepler* has the potential to measure the gravitational quadrupoles of very hot Jupiters though the technique described below. If successful, this will constitute a major step towards an understanding of the diversity of planetary interiors.

In Section 2, we describe the background theory that connects interior structure and orbital dynamics and explore which effects are most important. Section 3 applies this theory to the observable changes in the transit photometry, including full *Kepler* simulated light curves. We show in Section 4 that the signal due to the planetary interior has a unique signature. Other methods for inferring planetary interior properties are discussed in Section 5. The final section discusses the important conclusions of our work.

2.2 Background Theory

2.2.1 Coordinate System and Notation

The internal structure of very hot Jupiters can be determined by observing changes in the planet's orbit. These changes can be described in terms of two general types of precession. Apsidal precession refers to rotation of the orbital ellipse within the plane of the orbit. It is characterized by circulation

of the line of apsides, which lies along the major axis of the orbit. Nodal precession, on the other hand, occurs out of the plane of the orbit and refers to the orbit normal precessing about the total angular momentum vector of the system. For typical very hot Jupiter systems with no other planets, apsidal precession has a much stronger observable signal than nodal precession (see Section 2.4.1), so we focus our discussion on the simpler case of a fixed orbital plane.

As is typical for non-Keplerian orbits, the star-planet orbit is described using osculating orbital elements that change in time. We identify the plane of the sky as the reference plane and orient the coordinate axes in the usual way such that the sky lies in the x-z plane with the y-axis pointing at Earth. The intersection of the orbital plane and the reference plane is called the line of nodes, but without directly resolving the system, there is no way to determine the orientation of the line of nodes with respect to astronomical North; thus, the longitude of the ascending node, Ω, cannot be determined. Given this degeneracy, we simplify the description by orienting the z-axis to lie within the plane spanned by the orbit normal and the line-of-sight. The angle between the line of sight and the orbit normal is i, the inclination. The x-axis is in the plane of the sky and is the reference line from which the argument of periapse (ω) is measured (in the standard counter-clockwise sense). For this choice of coordinates, the argument of periapse and longitude of periapse (ϖ) are equivalent. Given this coordinate system, transit centers occur when the planet crosses the y-z plane; this point lies 90° past the reference x-axis, and thus primary transits occur when the true anomaly, f, satisfies $f_{tr} + \omega_{tr} \equiv 90°$, where the subscript tr indicates the value at transit center.[1]

Throughout this paper, we refer to parameters of the star (mass, radius, etc.) with subscripts of "$*$" and parameters of the planet with subscripts of "p". For evaluation of various equations, we will take as fiducial values the mass ratio $M_p/M_* = 10^{-3}$, the radius ratio $R_p/R_* = 0.1$ (though some low density planets have radius ratios greater than 1/6), and the semi-major axis in stellar radii $a/R_* = 6$, typical for very hot Jupiters, which we define as planets with semi-major axes $a \lesssim 0.025$ AU (see Table 1).[2] In this definition, we deviate from Beatty & Gaudi (2008), who define very hot Jupiters as planets with periods less than 3 days. These authors estimate that *Kepler* will find ∼30 such planets, of which ∼16 will be brighter than V=14 (T. Beatty, pers. comm.). Since our definition is more stringent, our technique will be applicable to fewer *Kepler* planets.

2.2.2 Rotational and Tidal Potentials

It is well known from classical mechanics, that if stars and planets are considered to be purely spherical masses, then they will obey a simple r^{-2} force law and hence execute closed elliptical orbits. Non-spherical mass effects are caused by the application of external potential(s): the centrifugal potential of spinning bodies causes rotational flattening and the tidal potential of a nearby mass

[1] In elliptical orbits, if the inclination is not 90°, the photometric minima do not exactly coincide with the planetary conjunctions. See Kopal (1959), p. 388 and section 2.3.3 below.

[2] Throughout this work, we do not distinguish between M_{tot} and M_*, since $M_p \ll M_*$.

raises tidal bulges. Rotational and tidal bulges create gravitational quadrupole fields (r^{-3}) that lead to orbital precession.

The complex subject of how planets[3] respond to applied potentials is encapsulated in the so-called theory of figures (Zharkov & Trubitsyn, 1978). As long as the distortions are small, we can simplify the problem by ignoring the small interaction terms between the tidal and rotational potentials; in this paper, we thus restrict ourselves to the first order theory, where the two planetary responses simply add. Even in the linear case, the way the fluid planet responds depends on the full radial density structure of the planet. The planetary response is conveniently captured in a single variable k_{2p}, using the definition

$$V_2^{\rm ind}(R_p) \equiv k_{2p} V_2^{\rm app}(R_p) \tag{2.1}$$

where k_{2p} is the Love number of the planet, which is just a constant of proportionality between the applied second degree potential field $V_2^{\rm app}$ and the resulting field that it induces $V_2^{\rm ind}$ at the surface of the planet. Due to the orthogonality of the Legendre polynomials used to express the gravity field, if the planet is responding to a second degree harmonic field, then only the second degree harmonic of the planet's gravity field is altered, to first-order. Thus, k_{2p} is a measure of how the redistribution of mass caused by the applied potential actually affects the external gravity field of the planet. In the stellar literature, the symbol k_2 is used for the apsidal motion constant, which is half of the secular/fluid Love number that we use throughout this paper (Sterne, 1939a).

The Love number k_2 is an extremely useful parameterization, as it hides the complex interactions of a planet and an applied potential in just a single number. The process of calculating k_2 of a fluid object (like stars and gas giants), from the interior density distribution is fairly straightforward and outlined in several places (e.g., Sterne, 1939a; Kopal, 1959). Objects with most of their mass near their cores, like stars, have very low k_2 values ($\sim$0.03 for main sequence solar-like stars, Claret, 1995) since the distorted outer envelope has little mass and therefore little effect on the gravity field. Planets have much flatter density distributions, and thus distortions of their relatively more massive outer envelopes greatly affect the gravity field. At the upper extreme lies a uniform density sphere, which has $k_2 = 3/2$. In this way, k_2 *can be thought of as a measure of the level of central condensation of an object*, with stronger central condensation corresponding to smaller k_2.

By examining the variations in k_2 for giant planets within our own Solar System, we can gain a feel for its expected values and how sensitive it is to internal structure. The $n = 1$ polytrope is commonly used to approximate the density structure of (cold) gas giant planets; it has $k_2 \approx 0.52$ (Kopal, 1959). This can be compared to the value determined from the gravity measurements of Jupiter, where $k_{2J} \simeq 0.49$. Even though Jupiter may have a 10 Earth mass core, it is small in comparison to Jupiter's total mass, and thus it has minor effect on the value of k_2. Saturn, on the

[3]For clarity, in these sections we focus on the planetary shape, though the derivations are also valid for stars.

other hand has a roughly 20 Earth mass core and is less than 1/3 of Jupiter's mass. As a result, the presence of Saturn's core is easily seen in the value of its Love number $k_{2S} \approx 0.32$. From this, we can see that planets with and without significant cores differ in k_{2p} by about ~ 0.1. This can also be inferred from Barnes & Fortney (2003) by using the Darwin-Radau relation to convert the moment of inertia factor to k_2. Furthermore, Bodenheimer et al. (2001) list the moment of inertia factors of various planet models of HD 209458 b and τ Bootis b, which correspond to a range of k_{2p} values from $\sim$0.1 to $\sim$0.6.

Current methods for inferring the internal structures of extra-solar planets combine measurements of the mass and radius with a model to obtain estimates of the planet's implied composition and core size. Unfortunately, these models require one to make assumptions about the degree of differentiation, among other things (Baraffe et al., 2008). A good measurement of k_{2p}, however, reveals important independent structure information, which can break the degeneracies between bulk composition and the state of differentiation. Given such a wide range of potential k_{2p} values, even an imprecise measurement of k_{2p} will be extremely valuable for understanding extra-solar planets. By measuring the k_{2p} values for extra-solar planets, we can also uncover constraints on the density structure that are independent of the measurement of the planetary radius. This new information may allow us to probe the unknown physics responsible for the currently unexplained radius anomalies.

2.2.2.1 Induced External Gravity Field

The internal structures of planets in our own solar system are most readily characterized by the zonal harmonics of the planet's gravity field, i.e., J_2, J_4, etc. It is these high-order harmonics that are directly measured by spacecraft flybys. To better understand the connection between the two, we can relate the k_2 formulation to J_2 by writing out the expression for the induced potential at the surface of the planet in Equation 2.1 in terms of the definition of J_2, yielding: $k_{2p} V_2^{\rm app}(R_p) = -J_2 \frac{GM_p}{R_p} P_2(\cos\theta)$, where P_2 is the usual Legendre polynomial and θ is the planetary co-latitude (Murray & Dermott, 1999). We can use this equation to obtain expressions for the J_2 field induced by both rotation and tides (discussed in more detail below). The relation relies on dimensionless constants which compare the strength of the acceleration due to gravity with that of the rotational and tidal potentials:

$$q_r = \frac{\nu_p^2 R_p^3}{GM_p} \qquad \text{and} \qquad q_t = -3\left(\frac{R_p}{r}\right)^3 \left(\frac{M_*}{M_p}\right) \tag{2.2}$$

where ν_p is the angular spin frequency of the planet. For the case where the spin axis and tidal bulge axis are perpendicular (i.e., zero obliquity), the relationship between J_2 and k_2 is, to first order:

$$J_2 = \frac{k_2}{3}\left(q_r - \frac{q_t}{2}\right) \tag{2.3}$$

Note that q_t is a function of the instantaneous orbital separation, r, and is thus constantly changing in an eccentric orbit in response to the changing tidal potential. Hence J_2 for eccentric extra-solar planets is a complex function of time. This is why it is more sensible to analyze the orbital precession in terms of k_2, which is a fixed intrinsic property of the planet, rather than J_2.

As very hot Jupiters are expected to be synchronously locked (denoted by s) with small eccentricities, it can easily be shown that $q_t^s \approx -3q_r$, which simplifies equation 2.3 yielding:

$$J_{2p}^s \simeq \frac{5}{6}k_{2p}q_r \simeq \frac{5}{6}k_{2p}\left(\frac{M_*}{M_p}\right)\left(\frac{R_p}{a}\right)^3 \tag{2.4}$$

Using a moderate value of $k_{2p} = 0.3$, the J_2 of very hot Jupiters reaches as high as 5×10^{-3}, about half of the measured J_2 of Jupiter and Saturn.

2.2.3 Apsidal Precession

The quadrupole field created by rotational and tidal potentials discussed above induces precession of the star-planet orbit. Both Jupiter and Saturn have rather significant quadrupoles, dominated entirely by their sizeable rotational bulges resulting from rapid rotation periods of less than 10 hours. In contrast, very hot Jupiters are expected to be synchronously rotating, and thus their spin periods are longer by a factor of a few. Since the rotational bulge size goes as the square of the spin frequency, very hot Jupiters should have rotational bulges that are at least an order of magnitude smaller than Jupiter and Saturn, inducing only tiny quadrupole fields. These extra-solar planets are extremely close to their parent stars, however, with semi-major axes of only ~ 6 stellar radii. Very hot Jupiters are thus expected to have large tidal bulges which are shown below to dominate the quadrupole field and resulting apsidal precession.

2.2.3.1 Precession Induced by Tidal Bulges

The orbital effect of tidal bulges is complicated by their continuously changing size. While tidal bulges always point directly[4] at the tide-raising object, their size is a function of orbital distance. Since the height of the tidal bulge depends on the actual separation between the objects, the second-order gravitational potential is time-varying in eccentric orbits. Accounting for this dependence (which cannot be captured by using a fixed J_2) is critical, as illustrated by Sterne (1939a). The

[4]We can ignore the lag due to dissipation, which has an angle of only $Q_p^{-1} \lesssim 10^{-5}$ for giant planets (Goldreich & Soter, 1966; Murray & Dermott, 1999).

dominant tidal perturbation to the external gravity field of the planet, evaluated at the position of the star, is a second-order potential:

$$V_{tid}(r) = \frac{1}{2} k_2 G M_* R_p^5 r^{-6} \tag{2.5}$$

The apsidal precession due to the tidal bulge, including the effect of both the star and the planet is (Sterne, 1939a; Eggleton & Kiseleva-Eggleton, 2001):

$$\begin{aligned} \dot{\omega}_{\rm tidal} &= \dot{\omega}_{\rm tidal,*} + \dot{\omega}_{\rm tidal,p} \\ &= \frac{15}{2} k_{2*} \left(\frac{R_*}{a} \right)^5 \frac{M_p}{M_*} f_2(e) n \\ &+ \frac{15}{2} k_{2p} \left(\frac{R_p}{a} \right)^5 \frac{M_*}{M_p} f_2(e) n \end{aligned} \tag{2.6}$$

where n is the mean motion and $f_2(e)$ is an eccentricity function:

$$\begin{aligned} f_2(e) &= (1-e^2)^{-5} (1 + \frac{3}{2} e^2 + \frac{1}{8} e^4) \\ &\approx 1 + \frac{13}{2} e^2 + \frac{181}{8} e^4 + ... \end{aligned} \tag{2.7}$$

Note that the factor of 15 does not appear for stationary rotational bulges, as detailed below, and comes through Lagrange's Planetary Equations from the higher dependence on radial separation (r^{-6}) in the tidal potential. For this reason, tidal bulges are much more important in producing apsidal precession.

Furthermore, the main factor of importance to extra-solar planets is the mass ratio, which comes in because the height of the tide is proportional to the mass of the tide-raising body. Consider the ratio of the planetary and stellar effects:

$$\frac{\dot{\omega}_{\rm tidal,p}}{\dot{\omega}_{\rm tidal,*}} = \frac{k_{2p}}{k_{2*}} \left(\frac{R_p}{R_*} \right)^5 \left(\frac{M_*}{M_p} \right)^2 \simeq 100 \tag{2.8}$$

For tidal bulges, the apsidal motion due to the planet clearly dominates over the contribution of the star. Even though the planet's radius is smaller than the star's by a factor of ten, the star is so much more massive than the planet that it raises a huge tidal bulge, which consequently alters the star-planet orbit. The benefit provided by the inverse square of the small mass ratio is compounded by the order of magnitude increase in k_2 of the planet over the star.

2.2.3.2 Precession Induced by Rotational Bulges

The quadrupolar gravitational field due to the planetary rotational bulge, evaluated at the star's position is:

$$V_{\rm rot}(r) = \frac{1}{3} k_2 \nu_p^2 R_p^5 r^{-3} P_2(\cos\alpha_p) \tag{2.9}$$

where α_p is the planetary obliquity, the angle between the orbit normal and the planetary spin axis. Sterne (1939a) assumes zero obliquity and calculates the secular effect of this perturbation on the osculating Keplerian elements. This final result, including the effect of both the star and the planet is[5]:

$$\begin{aligned} \dot{\omega}_{\rm rot} &= \dot{\omega}_{\rm rot,*} + \dot{\omega}_{\rm rot,p} \\ &= \frac{k_{2*}}{2}\left(\frac{R_*}{a}\right)^5 \frac{\nu_*^2 a^3}{GM_*} g_2(e) n \\ &+ \frac{k_{2p}}{2}\left(\frac{R_p}{a}\right)^5 \frac{\nu_p^2 a^3}{GM_p} g_2(e) n \end{aligned} \tag{2.10}$$

where $g_2(e)$ is another eccentricity function:

$$g_2(e) = (1-e^2)^{-2} \approx 1 + 2e^2 + 3e^4 + ... \tag{2.11}$$

Evaluating the importance of this effect requires an understanding of the spin states of very hot Jupiters and their stars. The rotation and spin pole orientation of very hot Jupiters should be tidally damped on timescales $\lesssim 1$ MYr (e.g., Dobbs-Dixon et al., 2004; Ferraz-Mello et al., 2008). We therefore assume that all planets have reached the psuedosynchronous rotation rate derived by Hut (1981). The rotation rate of the star is usually much slower since the tidal stellar spin-up timescale is much longer than $\sim$1 GYr (Fabrycky et al., 2007).

If both the star and the planet were spinning synchronously, the stellar and planetary rotational bulges would have comparable contributions to apsidal precession. However, since the tidal bulge of the planet is a much more important effect, we find that even fast-spinning stars have a very weak contribution to apsidal precession.

2.2.3.3 Total Apsidal Precession

The other major contributor to the apsidal precession in extra-solar planetary systems is general relativity. The anomalous apsidal advance of Mercury's orbit due to its motion near the massive Sun was one of the first confirmations of general relativity. This same apsidal advance is prevalent in very hot Jupiter systems and has been shown to be possibly detectable through long-term transit

[5]The full equation, including arbitrary obliquities, is given in Kopal (1978), Equation V.3.18 (see also Sterne, 1939a; Eggleton & Kiseleva-Eggleton, 2001). Also recall that, unlike these authors, we use the symbol k_2 to represent the Love number which is twice the apsidal motion constant called k_2 in eclipsing binary literature.

timing (Miralda-Escudé, 2002; Heyl & Gladman, 2007; Pál & Kocsis, 2008; Jordan & Bakos, 2008). The relativistic advance is given (to lowest order) by:

$$\dot{\omega}_{GR} = \frac{3GM_* n}{ac^2(1-e^2)} \tag{2.12}$$

One additional effect for non-synchronous planets is due to thermal tides (Arras & Socrates, 2009), which create a bulge on the planet due to temperature-dependent expansion of an unevenly-radiated upper atmosphere. The thermal tidal bulge is very small in mass and is not expected to provide a significant contribution to apsidal precession (P. Arras, pers. comm.) and is thus neglected.

Since we are considering only the lowest-order effects, all the apsidal precession rates (rotational/tidal for the star/planet and general relativity) simply add to give the total apsidal precession (roughly in order of importance for very hot Jupiters):

$$\dot{\omega}_{\rm tot} = \dot{\omega}_{\rm tid,p} + \dot{\omega}_{\rm GR} + \dot{\omega}_{\rm rot,p} + \dot{\omega}_{\rm rot,*} + \dot{\omega}_{\rm tid,*} \tag{2.13}$$

We are ignoring the small cross-terms (geodetic precession, quadrupole-quadrupole coupling, Lense-Thirring effect, nutation, etc.) for the purposes of this paper as higher-order corrections.

Calculating each of these contributions to the precession shows that *for very hot Jupiters, the dominant term in the total apsidal precession is due to the planetary tidal bulge.* For the known transiting planets, the fraction of apsidal precession due to the planet is calculated and illustrated in Figure 1. The precession due to the interiors of very hot Jupiters towers over the other effects. General relativity, the next largest effect is ∼10 times slower than the precession caused by the planetary tidal bulge.

The apsidal precession rate of very hot Jupiters due solely to the interior structure of the planet is:

$$\begin{aligned} \dot{\omega}_{\rm p} \quad &\approx \quad 3.26 \times 10^{-10} \text{ rad/sec } \times \left(\frac{k_{2p}}{0.3}\right) \left(\frac{M_*}{M_\odot}\right)^{3/2} \times \\ &\left(\frac{M_p}{M_{\rm J}}\right)^{-1} \left(\frac{R_p}{R_{\rm J}}\right)^{5} \left(\frac{a}{0.025 \text{ AU}}\right)^{-13/2} \end{aligned} \tag{2.14}$$

which explains why low density very close-in Jupiters are the prime targets for measuring apsidal precession. For these planets, the precession rate can reach a few degrees per year.

The precession due to the planet has generally been neglected in extra-solar planet transit timing work to date (Miralda-Escudé, 2002; Heyl & Gladman, 2007), which has considered stellar oblateness or general relativity to be the dominant effects (in the absence of other planets) though Jordan & Bakos (2008) have also pointed out that $\dot{\omega}_{\rm tidal,p}$ can be an important source of apsidal precession. We

find that the planetary quadrupole is usually 1-2 orders of magnitude more important than effects previously considered for single very hot Jupiters. Hence, measuring apsidal precession essentially gives $\dot{\omega}_{\rm tid,p}$ which is directly proportional to k_{2p}, implying that transit light curve variations due to apsidal precession can directly probe the interiors of extra-solar planets.

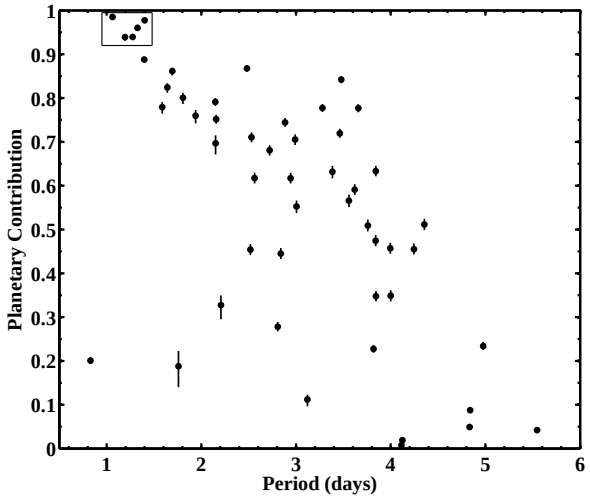

Figure 2.1
Fraction of Apsidal Precession Due to the Planetary Quadrupole. The points show the planetary fraction of the total apsidal precession calculated for the known transiting extra-solar planets with properties taken from J. Schneider's Extra-Solar Planet Encyclopedia (`http://www.exoplanet.eu`), assuming the planet has a typical Love number of $k_{2p} = 0.3$ (e.g. Saturn-like). The apsidal precession induced by the tidal and rotational bulges of the planet overcome precession due to general relativity and the star, especially for short period planets. The "error bars" show the range of planetary contributions for a 5% variation in stellar masses (and hence $\dot{\omega}_{\rm GR}$) and the comparatively smaller effect of varying the stellar Love number and rotation rate over all reasonable values. The five cases where the planetary contribution to apsidal precession is most important (boxed) also have the shortest precession periods: WASP-12b, CoRoT-1b, OGLE-TR-56b, WASP-4b, and TrES-3b would fully precess in about 18, 71, 116, 120, and 171 years, respectively. The planet in the lower left is CoRoT-7, a super-Earth planet whose planetary contribution to precession is small because of its small radius. Transiting planets with periods longer than 6 days all had planetary contributions less than 0.15. In all cases, the dominant signal in apsidal precession of very hot Jupiters is k_{2p}, which is determined by their internal density distribution and is a powerful probe into their interior structure.

2.2.4 Modification of the Mean Motion

Non-Keplerian potentials also modify the mean-motion, n, and cause a small deviation from Kepler's Third Law. Including the effects described above, the non-Keplerian mean motion, n', is (dropping second-order corrections):

$$n' = n\left(1 + \epsilon - \frac{3GM_*}{2ac^2}\right) \tag{2.15}$$

where ϵ is defined as

$$\begin{aligned} \epsilon &= \frac{k_{2*}}{2} q_{r,*} \left(\frac{R_*}{a}\right)^2 + \frac{k_{2p}}{2} q_{r,p} \left(\frac{R_p}{a}\right)^2 \\ &+ 3k_{2*}\frac{M_p}{M_{tot}}\left(\frac{R_*}{a}\right)^5 + 3k_{2p}\frac{M_*}{M_p}\left(\frac{R_p}{a}\right)^5 \end{aligned} \tag{2.16}$$

and $n^2 \equiv \frac{GM_{tot}}{a^3}$. The general relativistic correction to the mean motion is from Soffel (1989). (Throughout this paper, except where noted, the difference between n' and n is ignored as a higher-order correction.)

As with apsidal precession, the planetary quadrupole is more important than the stellar quadrupole by about 2 orders of magnitude. At the largest, the correction to the mean motion is a few times 10^{-5}. Iorio (2006) used the fact that quadrupole moments cause deviations to Kepler's Third Law to attempt to derive the J_2 of the star HD 209458 (the quadrupole of the planet was incorrectly ignored).

However, as Iorio (2006) found, this method is only feasible if you know the masses and semi-major axes of the orbit *a priori* or independently from Kepler's Law. Since the error in stellar masses (from radial velocities and evolutionary codes) is usually 3-10 % (e.g., Torres et al., 2008), the propagated error on k_{2p} would be a few times greater than the highest k_{2p} expected, making this method impractical. It has been proposed that the stellar mass and semi-major axis can be precisely and independently measured via the light-travel time effect described by Loeb (2005). In practice, however, the light-travel time effect is highly degenerate with the unknown transit epoch and/or the orbital eccentricity. We find that a precise independent measurement of M_* from light-travel time is impractical even with the excellent photometry of *Kepler*.[6]

2.2.5 Expectations for Planetary Eccentricities

Thus far, we have quantified how planetary interiors affect the orbit through precession. The photometric observability of this apsidal precession is highly dependent on the current orbital eccentricity (e). Small eccentricities are the largest limitation to using transit light curves to probe extra-solar

[6]We do note that detailed observations of multiple-planet systems can yield mass estimates of each of the bodies independently. *Kepler* asteroseismology can also provide independent information about stellar mass and other properties (Kjeldsen et al., 2008).

planet interiors. Indeed, if eccentricities are very low, measuring apsidal precession from transit light curves may not be possible for any of the *Kepler* planets.

Nearly all hot Jupiters have eccentricities consistent with zero, though the radial velocity technique has difficulty putting 3-σ upper limits on eccentricities smaller than 0.05 (Laughlin et al., 2005). So far, the strongest constraints are placed by comparing the deviation of the secondary transit time from half the orbital period, which are related by (e.g., Charbonneau et al., 2005):

$$e\cos\omega \simeq \frac{\pi}{2P_{\rm orb}}(t_{\rm sec} - t_{\rm prim} - \frac{P_{\rm orb}}{2}) \tag{2.17}$$

Similarly, by measuring the primary and secondary transit durations (Θ_I and Θ_{II}), an additional constraint can be placed on $e\sin\omega$. The equation commonly quoted in the extra-solar planet literature (Kallrath et al., 1999; Charbonneau, 2003; Winn et al., 2006) has a sign error; the correct equation is derived by Kopal (1959), p. 391 :

$$e\sin\omega = \frac{\Theta_{II} - \Theta_I}{\Theta_{II} + \Theta_I}\frac{\alpha^2 - \cos^2 i}{\alpha^2 - 2\cos^2 i} \tag{2.18}$$

where $\alpha \equiv \frac{R_* + R_p}{a\sqrt{1-e^2}}$. The accuracy of this measurement is typically smaller than for $e\cos\omega$, but we include this equation to note that there is information about both the eccentricity and its orientation in the full transit light curve (see also Bakos et al., 2009).

Combining secondary transit timing information with radial velocity and Rossiter-McLaughlin measurements to help constrain ω, Winn et al. (2005) found the best-fit eccentricity for HD 209458 was $\sim$0.015. Though Winn et al. (2005) argue that the actual eccentricity is probably less than 0.01, it is not necessarily 0 (Mardling, 2007). Recently, Joshi et al. (2008) revealed WASP-14b, a young massive hot Jupiter with an eccentricity of 0.1; WASP-10b and WASP-12b also appear to be eccentric (Christian et al., 2008; Hebb et al., 2009), though these eccentricities may be spurious or overestimated.

The most accurate eccentricity constraint is a detection by Knutson et al. (2007a) for the very hot Jupiter HD189733b. They observed continuously and at high cadence (0.4 seconds) with the Spitzer space telescope and measured a secondary timing offset corresponding to $e\cos\omega = 0.001 \pm 0.0002$, a 5-$\sigma$ result that they could not explain by any other means. (Preliminary analysis of additional data for this planet by Agol et al. (2009) indicates $e\cos\omega = 0.0002 \pm 0.0001$.) The constraint on $e\sin\omega$ is much weaker. A non-zero eccentricity of $e \simeq 0.003$ for hot Jupiters is therefore consistent with every measurement available in the literature, though the actual values of eccentricities at the 10^{-3} level are essentially unconstrained.

In the absence of excitation, the current eccentricities of these planets depend on the initial eccentricity and the rate of eccentricity decay. Extrapolating from planets in our solar system

(Goldreich & Soter, 1966) implies short circularization timescales of $\simeq 10$ MYr, though recent studies have shown that using a fixed eccentricity damping timescale is an inappropriate simplification of the full tidal evolution (e.g., Jackson et al., 2008; Levrard et al., 2009; Rodriguez & Ferraz-Mello, 2009). Even an analysis using the full tidal evolution equations cannot give a compelling case for the present-day eccentricities of these planets, since there are essentially no direct constraints on the tidal dissipation parameter for the planet, Q_p. Various estimates show that Q_p for exoplanets is not known and may be quite large (e.g., Matsumura et al., 2008), implying that non-zero eccentricities are not impossible. Even so, we stress that the best candidates for observing apsidal precession are also those planets that have the fastest eccentricity damping, since the damping timescale and apsidal precession rates are both proportional to $\frac{M_p}{M_*}\left(\frac{a}{R_p}\right)^5$. Hence, those planets which have the fastest precession rates will also have the lowest eccentricities. The first step in determining if this trade-off allows for apsidal precession to be measured by *Kepler* data is to apply the techniques described in this paper to the data themselves. Furthermore, with the discovery and long-term characterization of more planets using ground and space-based observations, the detectability of apsidal precession will increase dramatically.

We should note that there are several mechanisms that can excite eccentricities and compete with or overwhelm tidal dissipation. The most prevalent is assumed to be eccentricity pumping by an additional companion (Peale et al., 1979; Bodenheimer et al., 2001; Adams & Laughlin, 2006). Even very small (Earth-mass or less) companions in certain orbits can provide significant eccentricity excitation (Mardling, 2007). (In this case, however, our single-planet method for estimating k_{2p} would need to be modified considerably.) Tidal dissipation in rapidly rotating stars tends to increase the eccentricity, potentially prolonging circularization in some systems (Ferraz-Mello et al., 2008). Very distant inclined companions (e.g., a planet orbiting a star in a misaligned binary star system) can induce Kozai oscillations that impart very large eccentricities on secular timescales (e.g., Fabrycky & Tremaine, 2007). Arras & Socrates (2009) proposed that thermal tides can significantly affect the orbital and rotational properties of extra-solar planets, though their conclusions appear to be overestimated (Goodman, 2009; Gu & Ogilvie, 2009). Finally, recent (not necessarily primordial) dynamical instabilities in the planetary system can also be responsible for generating eccentricity which simply hasn't damped away yet (Ford et al., 2005; Gomes et al., 2005; Chatterjee et al., 2007; Thommes et al., 2008). We, therefore, continue our analysis under the possibility that some very hot Jupiters may have non-zero eccentricities.

2.3 Transit Light Curves of Apsidal Precession

Previous studies of transit light curve variability due to non-Keplerian perturbations have focused almost exclusively on transit timing. In contrast, we model the full photometric light curve in order

to estimate the detectability of k_{2p}. This will automatically include the effect of changing transit durations, which are very useful for detecting apsidal precession (Pál & Kocsis, 2008; Jordan & Bakos, 2008). In addition, using full photometry can provide a more direct and realistic estimate of the detectability of k_{2p}. Of course, the drawback is additional computational cost, though we found this to be manageable, requiring less than 20 seconds to generate the ~ 2 million photometric measurements expected from *Kepler*'s 1-minute cadence over 3.5 years.

2.3.1 Our Transit Light Curve Model

Determining the photometric light curve of a transiting system requires knowing the relative positions of the star and the planet at all times. These can be calculated by describing the motion of the planet with time-varying osculating orbital elements. When describing the motion of the planet using instantaneous orbital elements, it is usually customary to ignore the periodic terms by averaging, as in Sterne (1939a), and calculate only the secular terms. These small periodic terms describe how the orbital elements change within a single orbit as a function of the true anomaly, f, due to the non-Keplerian potential. In precessing systems, the value of the true anomaly at central transit, $f_{tr} \equiv 90^\circ - \omega_{tr}$, changes subtly from one transit to the next, inducing slow variations in the osculating orbital elements at transit. Therefore, we include in our model the dominant periodic changes in orbital elements as a function of orbital phase, using $M_{tr} \approx f_{tr}$ as an appropriate approximation for low eccentricities. Using a direct integration (described in Section 2.4.1), we verified that ignoring these periodic variations can cause non-negligible systematic errors in determining transit times. The periodic changes are derived from the same disturbing potentials used above. We follow the method of Kozai (1959) for calculating osculating elements from mean elements, and assume zero obliquity. The correction is similar to the correction to the mean motion, which is also applied in our model. The correction to the semi-major axis, eccentricity, longitude of periapse, and mean anomaly are $a_{\rm osc} = a_{\rm mean} + \frac{2ae}{1-e^2}\epsilon \cos M \approx 2ae\epsilon \cos M$, $e_{\rm osc} = e_{\rm mean} + \epsilon(1 - \cos M)$, $\omega_{\rm osc} = \omega_{\rm mean} + \frac{\epsilon}{e}\sin M$, and $M_{\rm osc} = M_{\rm mean} - \frac{\epsilon}{e}\sin M$ where ϵ is defined in Equation 2.16. General relativistic periodic corrections are also added; these are taken from Soffel (1989), page 92 (with $\alpha = 0$, $\beta = \gamma = 1$). Using our direct integrator (described below), we verified that these corrections reproduced the actual orbit to sufficient accuracy for this analysis as long as $e \gg \epsilon \sim 10^{-5}$. Other corrections are higher order in small parameters and are ignored.

Our model uses these corrected elements to generate astrocentric Cartesian coordinates for a specific system inclination and, for completeness, also includes the effect of light-travel time (Loeb, 2005) though we concur with Jordan & Bakos (2008) and Pál & Kocsis (2008) that the light-travel time change due to $\dot{\omega}$ is unimportant. The positions are then translated to photometric light curves using the quadratic limb-darkening code[7] described in Mandel & Agol (2002). *Kepler* data will have

[7]Available at `http://www.astro.washington.edu/ agol/transit.tar.gz`

enough signal-to-noise to justify using non-linear limb darkening laws (Knutson et al., 2007b), but we do not expect that this simplification will significantly alter our conclusions.

In addition, we include the photometry of the secondary eclipse. As suggested by López-Morales & Seager (2007), very hot Jupiters can reach temperatures exceeding 2000 K, where their blackbody emission at optical wavelengths is detectable by *Kepler*. This thermal emission is added to the reflected light of the planet, which appears to be small based on the low upper limit of the albedo of HD 209458b and TrES-3 measured by Rowe et al. (2007) and Winn et al. (2008), respectively. We find that in *Kepler*'s observing bandpass of 430-890 nm (Koch et al., 2006), thermal emission of very hot Jupiters can dominate over the weak reflected light. We estimate the depth of the secondary eclipse ($d_{\rm sec}$) in our simulated *Kepler* data by assuming that 1% of the light is reflected and the other 99% absorbed and reemitted as processed thermal blackbody emission from the entire planetary surface (day and night sides). To be conservative and to account for unmodeled non-blackbody effects, we divide the resulting planet/star flux ratio by 2 (Hood et al., 2008); the resulting depth of around 2×10^{-4} is consistent with the lower values of Burrows et al. (2008), the tentative measurement of the thermal emission from CoRoT-2b (Alonso et al., 2009), and the detection of secondary eclipse emission from OGLE-TR-56b (Sing & López-Morales, 2009). We note that the best candidates for detecting k_{2p} are those with small semi-major axes and large radii; these same planets have relatively large $d_{\rm sec}$ values (Table 1). Secondary eclipses are very useful for determining e and ω. We will also find that they can be important for observing apsidal precession.

Our model generates accurate photometry for an extra-solar planet undergoing apsidal precession. Several other small photometric effects have been discussed in the literature, which we do not include. Most of these effects are periodic (e.g., the reflected light curve) and therefore will not affect the long-term trend of precession. Care will need to be taken to ensure that slow changes due to parallax and proper motion, which should be quite small for relatively distant stars observed by *Kepler* (Rafikov, 2008; Scharf, 2007) or changes in the stellar photosphere (Loeb, 2008) are not significant. Non-Gaussian astrophysical noise of the star and other systematic noise should degrade the accuracy with which k_{2p} can be measured compared to our ideal photometry. The long-term variability of the star can be interpolated away or modeled (Lanza et al., 2009), though it is not clear how short-term variability will affect transit light curves at *Kepler*'s level of precision. On the other hand, complimentary observations (e.g., warm Spitzer, HST, radial velocities, JWST, etc.) should only enhance our understanding of the systems studied.

2.3.2 Accuracy of k_{2p} Measurement

With an accurate photometric model of apsidal precession, one could estimate the measurement accuracy of k_{2p} from *Kepler* data by carrying out a full Monte Carlo study of the inversion problem, going from realistic synthetic photometric data sets to a determination of all system parameters. In

this work, instead, we carry out a much simpler calculation which cannot provide strict one-sigma error estimates like the Monte Carlo analysis, but does give an indication of how well k_{2p} can be resolved given a large dataset.

We obtain this accuracy estimate by comparing a realistic precessing photometric model with $k_{2p} \neq 0$ to a base model with $k_{2p} = 0$. The base model is still undergoing very slow apsidal precession, induced by general relativity and k_{2*}. We calculate the effect of a non-zero k_{2p} value by subtracting the precessing model from the base model. (See Figures 2.2 and 2.4.) Then, by calculating the root-sum-square of the residual signal and comparing it to the photometric error on a single data point, we obtain a numerical measure of the relative signal induced by k_{2p}. The "signal-to-noise" ratio for the data set is therefore given by:

$$\frac{\mathrm{S}}{\mathrm{N}} \sim \frac{\sqrt{\sum_i (y_i - y_i^0)^2}}{\sigma} \tag{2.19}$$

where y_i and y_i^0 are the photometry model values for the k_{2p} test model and the base model, respectively, and σ is the photometric error. We use $\sigma = 1000$ parts per million (ppm) flux per 1-minute integration, corresponding to the expected noise of *Kepler* on a faint $V = 14$ star (Koch et al., 2006). Of the 30 planets with periods less than 3 days, 16 are expected to be brighter than $V \simeq 14$ (T. Beatty, pers. comm.) and we can reasonably expect some fraction of these to have orbits comparable to the planets modeled here.

Since our residual signal changes as a function of time, this is not a true signal-to-noise calculation; the distribution of values in time matters for a proper interpretation, but any distribution would yield the same effective $\frac{S}{N}$, and thus this construction is not capturing all of the details. Even so, it does provide a useful and reasonable rough estimate for detectability. In order to identify the resolution on the k_{2p} measurement, we search for the value of k_{2p} which yields a signal-to-noise of $\frac{S}{N} = 1$. This is reasonable since it represents the threshold value of k_{2p}, below which planetary induced precession cannot be distinguished in the data with the given errors. The threshold k_{2p} value can also be loosely thought of as an estimate of the 1-σ expected errors.

This is a realistic estimate only insofar as the residual signal $(y_i - y_i^0)$ is due only to k_{2p} and cannot be absorbed by any other parameters. Hence we seek to choose other parameters so as to minimize the residuals without changing k_{2p}. For most system parameters, this is accomplished by referencing the time to the center of the data set, and thus the difference between the signals grows similarly forward and backward in time as seen in Figures 2.2 - 2.5. The transit shapes in both models are equivalent at the center of the dataset as would be expected in an analysis of actual data.

Additionally, a major effect from changing the precession period is to alter the observed average period. When analyzing actual data, this would just be absorbed into a small adjustment to the

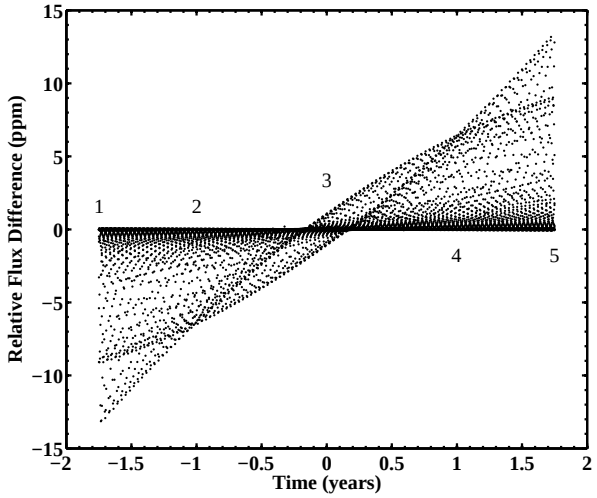

Figure 2.2 **Photometric Difference Signal from k_{2p}.** As described in the text, we use the difference between two theoretical light curves in the transit photometry to assess the observability of apsidal precession by *Kepler*. For WASP-4b at $\omega = 0°$, $e = 0.003$, and a central impact parameter, the difference between a model with $k_{2p} = 0$ and $k_{2p} = 0.146$ would yield an effective "signal-to-noise" of 1 on a moderately bright star ($V = 14$). Shown is this difference signal; the root sum of squares of the signal is equal to 1000 ppm, the expected photometric accuracy of *Kepler* for a 1 minute observation (Koch et al., 2006). The trends seen in the figure are illustrated in Figure 2.3 by considering excepts of single primary transits from the regions labeled 1-5.

(unknown) stellar mass, thereby adjusting the period to absorb much of the k_{2p} signal. It is therefore important to correct for the average period change to avoid significantly overestimating the signal due to k_{2p}. Additionally, there is a similar, though less severe, effect for the epoch of the first transit, which is also adjusted to best absorb signal. This is achieved by using an analytic expression for the transit times (see Equation 2.22 below) which match the transit times of the photometric model to very high accuracy. By fitting a line to these times, we can determine the average period and epoch that absorb the degenerate portions of the k_{2p} signal, leaving behind the residual due only to k_{2p}. We have not explicitly accounted for degeneracies between the signal from k_{2p} and the other parameters, like the radius, limb darkening, and system inclination, but since k_{2p} induces a time varying signal while these other parameters are generally constant, there is little expected signal absorption from these parameters.

The only major drawback of this approach is that it does not allow the eccentricity state of the system to change. With real data, the eccentricity and precession phase are not known in advance, and thus must be found by inversion. As detailed in Section 2.2.5, eccentricity and orbital orientation are primarily constrained by comparing primary and secondary transit pairs, and thus proper inversion is greatly aided by accurate observations in wavelengths more favorable to secondary transit observations, obtained by Spitzer, HST, or from the ground (e.g., Knutson et al., 2007a;

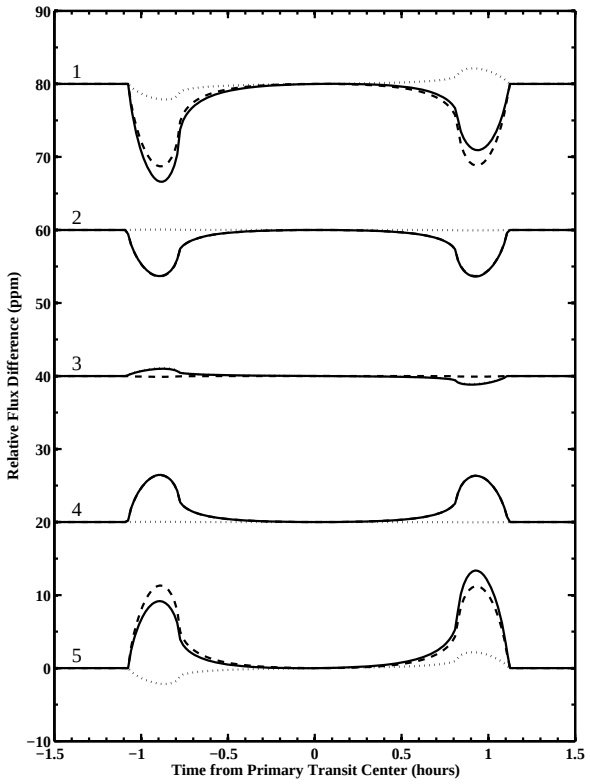

Figure 2.3 **Excerpts of Photometric Difference Signal.** Examining excerpts of the residual signal shown fully in Figure 2.2, the effects of transit timing and "transit shaping" can both be seen. The five excerpts are offset for clarity. Transit timing has an asymmetric signal (dotted lines), obtained when subtracting two transit curves slightly offset in time. Transit shaping, which is mostly due to changing transit duration, creates a symmetric signal (dashed lines). The total difference signal (solid lines) is dominated by the effect of transit shaping, which has ∼30 times more signal than transit timing alone. (See explanation in text.) Both effects are maximized at the beginning (1) and end (5), as expected for a signal that increases with longer baseline. The maximal signal occurs during ingress and egress, when the light curve changes the fastest. The transit shapes are equivalent at the center (3) by construction. The transit timing anomaly of precession is quadratic, which, when fitted with a best-fit straight line corresponding to a non-precessing signal, yields two intersections when transit timing is minimized (2,4). The transit timing offset at the beginning and end is only 0.085 seconds, while the center is offset by -0.042 seconds.

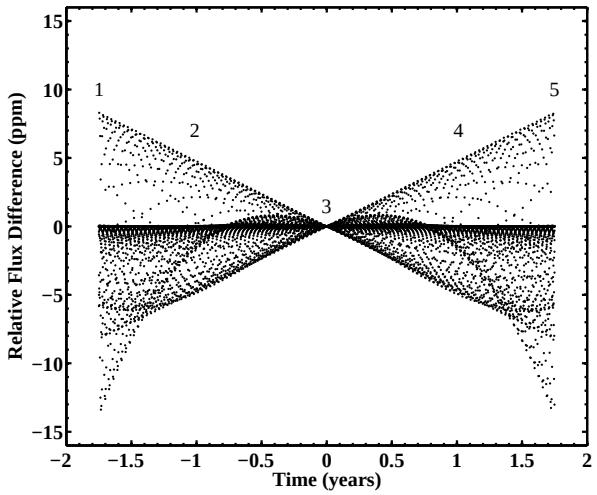

Figure 2.4 **Photometric Difference Signal from k_{2p}.** Similar to Figure 2.2, but for $\omega = 90°$. This figure is dominated by the photometric difference between secondary transits slightly offset in time. At $\omega = 90°$ the changes in the primary transits due to precession are small, except far away from the central time. At this orientation, the primary-secondary timing offset (Equation 2.17) is maximized. This "secondary transit timing" signal is weaker than the signal from primary transit as the secondary transit depth is much shallower. Therefore, an unreasonably high k_{2p} of 0.925 is required to detect the apsidal precession. Excerpts of single secondary transits taken from regions labeled 1-5 are shown in Figure 2.5.

Swain et al., 2008; Gillon et al., 2008). We also find that binned and folded *Kepler* data has comparable sensitivity to a single Spitzer observation for characterizing the secondary eclipses of very hot Jupiters. In any case, our assessment of the threshold k_{2p} assumes that the eccentricity of the system is very well known, which will likely require additional supporting observations.

2.3.3 Comparison to Expected Signal

The residual light curves calculated for each planet, Figures 2.2 - 2.5, match the theoretical expectations of the apsidal precession signal (Miralda-Escudé, 2002; Heyl & Gladman, 2007; Pál & Kocsis, 2008; Jordan & Bakos, 2008). To interpret the results of our analysis, it will be useful to briefly review the major components of the apsidal precession signal: changes in the times of primary transits, changes in the shape of primary transits, and changes in the primary-secondary offset times (Miralda-Escudé, 2002; Heyl & Gladman, 2007; Pál & Kocsis, 2008; Jordan & Bakos, 2008).

The primary transit times, T_N, due to apsidal precession are well described by a sinusoid for very low eccentricities ($e \ll 0.1$):

$$T_N = T_0 + NP_{\rm obs} + \frac{eP_{\rm obs}}{\pi}(\cos\omega_{tr,N} - \cos\omega_{tr,0})] \tag{2.20}$$

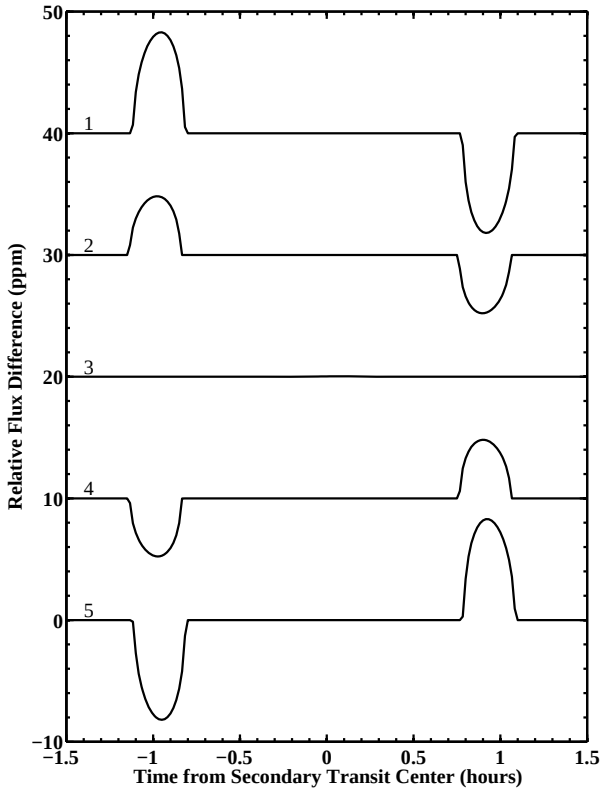

Figure 2.5 **Excerpts of Photometric Difference Signal.** Similar to Figure 2.3, but for $\omega = 90°$. Single secondary transit differences are excised from the full difference signal shown in Figure 2.4. The shape of the curves is due to the subtraction of two secondary transits slightly offset in time. Since the secondary transits are complete occultations, they are flat-bottomed and lack the additional structure due to limb-darkening seen in Figure 2.3. By construction, the offset grows in time away from the center (3) of the signal and attains a maximum at the beginning (1) and end (5). Curves 2 and 4 are shown for comparison to Figure 2.3.

where T_0 is the epoch of the first transit, $\omega_{tr,N} \equiv \dot{\omega}(T_N - T_0) + \omega_{tr,0}$ is the argument of periapse for the $N^{\rm th}$ transit, and $P_{\rm obs}$ is the *observed* period between successive transits, which deviates from the actual orbital period since the orbit has precessed a small amount between transits (Batten, 1973). For small eccentricities, the amplitude of the transit timing variations due to k_{2p} is:

$$\frac{eP_{\rm obs}}{\pi} \simeq 119 \text{ sec} \times \left(\frac{e}{0.003}\right)\left(\frac{a}{0.025 \text{ AU}}\right)^{3/2}\left(\frac{M_*}{M_\odot}\right)^{-1/2} \tag{2.21}$$

Given that individual transit times can be measured with accuracies of only a few seconds, even tiny eccentricities $e \lesssim 10^{-5}$ can induce detectable transit timing variations on precessional timescales ($\sim \dot{\omega}^{-1}$).

For our analysis, we extended Equation 2.20 to fifth order in eccentricity allowing accurate determination of transit times for eccentricities up to of order 0.1. We also require a correction for the effect of a non-central impact parameter ($i < 90°$, $e > 0$). For an inclined eccentric orbit, the apparent path of the planet across the stellar disk is curved. At orientations where the line of sight is not along the major axis of the ellipse, the curved path is also asymmetric. Therefore, the times of photometric minima, T_N, do not correspond exactly to the times of conjunction (when the planet crosses the $y - z$ plane and $f_{tr} \equiv 90° - \omega_{tr}$). We follow the correction from Equation VI.9-21 of Kopal (1959), who find that at photometric minimum, $f_{tr} = 90° - \omega'_{tr}$, where $\omega'_{tr} \equiv \omega_{tr} + e\cos\omega_{tr}\cot^2(i)(1 - e\sin\omega_{tr}\csc^2(i))$; in this corrective term, it is only required to keep terms up to second order in eccentricity. Assuming that i and $\dot{\omega}$ are constant, it can be shown that

$$\begin{aligned}
T_N &= T_0 + NP_{\rm obs} \\
&+ \frac{P_{\rm obs}}{\pi}\Bigg[e(\cos\omega'_{tr,N} - \cos\omega'_{tr,0}) \\
&+ \frac{3}{8}e^2(\sin 2\omega'_{tr,N} - \sin 2\omega'_{tr,0}) \\
&+ \frac{1}{6}e^3(\cos 3\omega'_{tr,N} - \cos 3\omega'_{tr,0}) \\
&+ e^4\Big(\frac{1}{16}(\sin 2\omega'_{tr,N} - \sin 2\omega'_{tr,0}) \\
&- \frac{5}{64}(\sin 4\omega'_{tr,N} - \sin 4\omega'_{tr,0})\Big) \\
&+ e^5\Big(\frac{1}{16}(\cos 3\omega'_{tr,N} - \cos 3\omega'_{tr,0}) \\
&- \frac{3}{80}(\cos 5\omega'_{tr,N} - \cos 5\omega'_{tr,0})\Big)\Bigg]
\end{aligned} \tag{2.22}$$

This transcendental equation is solved iteratively for $(T_N - T_0)$ to obtain the transit times and has been tested thoroughly against the empirical determination of transit times calculated by our light

curve model described above.

The expected apsidal precession periods (including small contributions from GR and the star) for WASP-12b, CoRoT-1b, OGLE-TR-56b, WASP-4b, and TrES-3b are around 18, 71, 116, 120, and 171 years, respectively. In other words, they have precession rates induced by the planetary tidal bulge of a few degrees per year, compared to a few degrees per century as the fastest general relativistic precession (Jordan & Bakos, 2008). We caution that if $\frac{R_p}{a}$ for WASP-12b is overestimated due to imprecise data (e.g., Winn et al., 2007), then the precession period would increase accordingly.

Even with such fast precession rates, the duration of observations will generally be much shorter than the precession period. In addition, as discussed above, the linear timing anomalies will be absorbed into the effective period as a small change in the unknown stellar mass (Heyl & Gladman, 2007; Pál & Kocsis, 2008; Jordan & Bakos, 2008). Therefore, detection of apsidal precession from primary transit times alone will require a significant detection of the curvature over a small portion of a long-period sinusoid. Since the curvature in Equation 2.20 is maximal at $\omega \approx 0, 180°$, these orientations have the best primary transit timing signal. Even at these orientations, detecting k_{2p} from primary transit times alone is difficult, since it can be shown that the signal strength is proportional to $e\dot{\omega}^2$, due to the need to detect curvature (Heyl & Gladman, 2007).

When the observational baseline is much shorter than the decades-long precession period, utilizing the changing shape of the transits can significantly improve detectability of apsidal precession (Pál & Kocsis, 2008; Jordan & Bakos, 2008). Transit shapes are primarily determined by the orbital speed at transit $\dot{f}_{tr}$ and impact parameter b, both of which depend on the precession phase ω_{tr}. For small eccentricities, the orbital angular speed at transit is given simply by $\dot{f}_{tr} \simeq n(1 + 2e\cos\omega_{tr})$. Changes in the impact parameter are somewhat more subtle, since b is given by $r_{tr}\cos i/R_*$, where $r_{tr} \simeq a(1-e^2)/(1+e\sin\omega_{tr})$ is the star-planet separation. Hence, the apparent impact parameter of the planet can change for non-central transits, even when the orbital plane remains fixed. The evolving transit shape of precessing orbits is determined by variations in both orbital speed and impact parameter. Simplifying the effect of transit shape by considering only the variations in transit duration as a function of ω_{tr}, Pál & Kocsis (2008) and Jordan & Bakos (2008) find that these two effects are of comparable magnitude. These authors also show analytically that the two effects exactly cancel when $b = 1/\sqrt{2}$. At this impact parameter, the transit duration stays constant throughout apsidal precession. The full photometric transit shape, however, still changes detectably in a precessing orbit, though the magnitude of signal is reduced (Figure 2.7).

The expected effect of changing transit shapes is fully consistent with the photometric difference signals calculated by our model (Figures 2.2 and 2.3). Indeed, our model shows that transit shaping dominates the signal by a factor of $\gtrsim$30 (Figure 2.3). We can also see that changes in the transit shape are maximized at orientations near $\omega \approx 0, 180°$ (as expected from Equation 2.18).

For small eccentricities, the transit shaping signal strength is given by $\frac{S}{N} \propto e\dot{\omega} \propto ek_{2p}$. Therefore,

when transit shaping dominates the observable signal, we should find that searching for the threshold k_{2p} value that yields $\frac{S}{N} = 1$ results in a power law relationship between threshold k_{2p} and e, such that $k_{2p} \propto e^{-1}$. By solving for threshold k_{2p} for eccentricities from 0.001 to 0.1, we find, as expected, that threshold k_{2p} very closely follows a power law in eccentricity with a slope of -1 for all planets. This power law relationship can be written as $ek_{2p} = C$, where C is a constant calculated from our model that depends on the planetary, orbital, and stellar parameters of the system.

At $\omega \approx 90, 270°$, transit timing and transit shaping effects are much weaker and are rather ineffective at constraining apsidal precession. At these orientations (when the Earth's line of sight is nearly aligned with the major axis of the orbit), another photometric signal emerges: variations in the difference between the times of primary and secondary transits. The changing orientation of the orbital ellipse causes a variation in the offset between primary and secondary transit times following Equation 2.17 above (Heyl & Gladman, 2007; Jordan & Bakos, 2008). These authors show that the strength of this signal is also proportional to $e\dot{\omega}$ and we find that the variation in threshold k_{2p} then also follows $k_{2p} \propto e^{-1}$.

The photometric difference signal at $\omega = 90°$ is shown in Figures 2.4 and 2.5. Using the method described in Section 2.3.2 to remove degeneracies almost eliminates the primary transit signal entirely, as expected, and the secondary transit offset becomes the more powerful signal. For WASP-12b, with an expected *Kepler* secondary transit depth of ∼1830 ppm, the threshold k_{2p} is actually *lower* at $\omega = 90°$ (Figure 2.6). For the other planets, the secondaries are not as important.

Our estimates of threshold k_{2p} at $\omega = 90°$ are based on the unknown secondary transit depth ($d_{\rm sec}$) in the *Kepler* bandpass (though our estimates of $d_{\rm sec}$ are consistent with all the measurements in the literature to date). Furthermore, we find that $\frac{S}{N} \propto d_{\rm sec}$, so that deeper secondary transits improve the accuracy with which k_{2p} can be measured. It is important to note that combining *Kepler* primary transit times with precise secondary transit times measured in the near-infrared (e.g., by warm Spitzer, HST, or JWST) is a very powerful way to constrain apsidal precession (Heyl & Gladman, 2007) for any orientation. Even a few high-precision secondary eclipse observations are enough to lower the value of threshold k_{2p} from our predictions, especially when $\omega \approx 90, 270°$.

By construction, threshold k_{2p} values vary linearly with the assumed photometric error $\sigma = 0.001 \times 10^{0.2(V-14)}$. In addition, re-performing our analysis using a 6-year long *Kepler* mission improved threshold k_{2p} values by a common factor of ∼2.2.

2.3.4 Results for Specific Planets

Using the method described above, we have determined the threshold k_{2p} for the most favorable known transiting planets as analogs for the very hot Jupiters to be discovered by *Kepler*. The threshold k_{2p} for each planet was computed at a range of eccentricities from 0.001 to 0.1 and for $\omega = 0°$ and $\omega = 90°$. Using the relationship discussed above ($k_{2p} \propto e^{-1}$) we interpolated (and

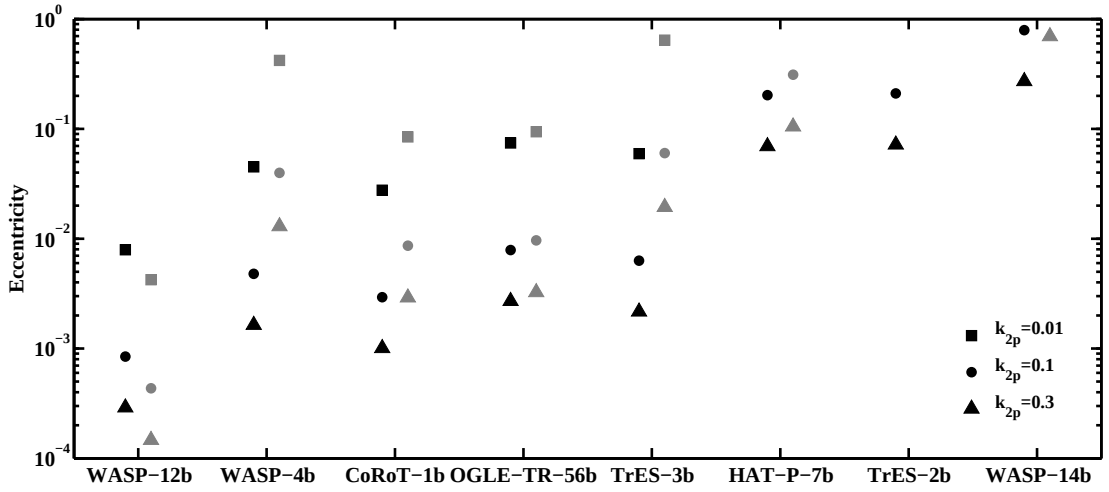

Figure 2.6 **Eccentricities Needed to Detect Interior Properties from Apsidal Precession.** The best-known planets for detecting k_{2p} precession are analogs to the hot Jupiters WASP-12b, WASP-4b, CoRoT-1b, OGLE-TR-56b, TrES-3b, HAT-P-7b, TrES-2b, and WASP-14b. Assuming that analogs to these planets exist in the *Kepler* field around a V=14 magnitude star, the above graph shows the eccentricities required to detect k_{2p}. Black symbols correspond to calculations with $\omega = 0°$ and gray symbols correspond to $\omega = 90°$; in both cases, $b = 0$. Apsidal precession is much easier to detect for larger eccentricities so increasing e decreases the detectable k_{2p}. Using our transit light curve model, we found that threshold k_{2p} values followed a power law $k_{2p} \propto e^{-1}$ (for low eccentricities), which is consistent with the analytical estimates that $\frac{S}{N} \propto e\dot{\omega} \propto ek_{2p}$ (see Section 2.3.2). Interpolating (and sometimes extrapolating) on this power law relationship, the graph identified the eccentricities required of these analog planets to detect precession due to a "typical" planetary interior of $k_{2p} = 0.3$ (triangles). For example, when $e = 0.00026$ and $\omega = 0°$, the apsidal precession due to an analog of WASP-12b should be just detectable by *Kepler*. A higher eccentricity (shown in Table 1) would be needed to measure k_{2p} with sufficient accuracy (0.1) to distinguish between a massive core and a core-less model (circles). Systematic errors are expected to become important once the measurement error on k_{2p} reaches as low as 0.01 (squares). If any of the very hot Jupiters discovered by *Kepler* have comparable eccentricities, the long-term high-precision photometry would allow for a powerful probe into their interior structure. HAT-P-7b and TrES-2b are known to lie in the *Kepler* observing field, but the values above are not corrected for improved photometric accuracy obtainable on these bright stars. Note that the eccentricities shown above and in Table 1 are computed for $\frac{S}{N} = 1$; 3-σ measurements require eccentricities 3 times as high.

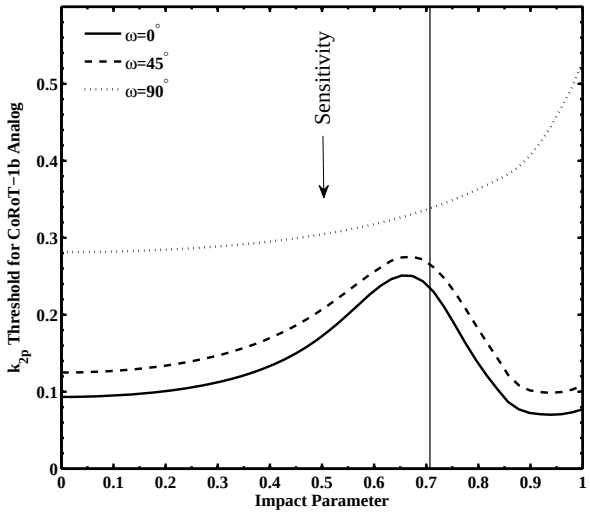

Figure 2.7 **Effect of Impact Parameter on Precession Signal.** The detectability of apsidal precession depends on the impact parameter (b) of the orbital track across the star. For $\omega = 0°$ (solid), the signal of primary transits are most important, with transit shaping playing the largest role. (See Figure 2.3.) However, the strength of transit shaping is a function of impact parameter with the minimum effect analytically estimated by Jordan & Bakos (2008) and Pál & Kocsis (2008) to be $b = 1/\sqrt{2}$ (vertical solid line). Using a full photometric model, we see the expected decrease in the shaping signal (i.e., requiring a larger k_{2p} to reach $\frac{S}{N} = 1$). Note that the signal is nearly maximal, with small threshold k_{2p} values, for a large range of impact parameters. When $\omega = 90°$ (dotted), the effect of primary transits are minimal and the offset in secondary transits become the determining factor. (See Figure 2.4.) At high impact parameters secondary eclipses are grazing, reducing the observable signal. We also show the threshold k_{2p} for an orientation of $\omega = 45°$, which lies, as expected, between the two extremes. The values of threshold k_{2p} shown are for an V=14 CoRoT-1b analog in the *Kepler* field with an eccentricity of 0.003.

Table 2.1. Extra-Solar System Parameters and Results

Planet Analog	M_* $M_\odot$	R_* $R_\odot$	M_p M_J	R_p R_J[a]	a AU	$d_{\rm sec}$[b] ppm	$\dot{\omega}_{tot}$ °/yr	e (Threshold k_{2p}=0.1)[c] $\omega = 0°$	$\omega = 90°$	Threshold $\dot{P}$[d] ms/yr	Thresh. Q_*[d]	Ref
WASP-12b	1.35	1.57	1.41	1.79	0.0229	1830	19.9	0.0008	0.0004	0.95	92700	1
CoRoT-1b	0.95	1.11	1.03	1.55	0.0245	314	4.96	0.0028	0.0085	0.93	12500	2,3
WASP-4b	0.92	0.91	1.24	1.36	0.0234	109	2.91	0.0047	0.0394	0.68	9900	4
TrES-3b	0.93	0.83	1.91	1.34	0.0228	106	2.04	0.0062	0.0614	0.53	13700	5
OGLE-TR-56b	1.17	1.32	1.29	1.30	0.0236	451	3.00	0.0077	0.0096	1.36	24700	6
HAT-P-7 b	1.47	1.84	1.77	1.36	0.0377	176	0.25	0.2085	0.3146	6.73	2800	7
TrES-2 b	0.98	1.00	1.19	1.22	0.0367	18	0.13	0.2102	... [e]	2.94	350	8
WASP-14b	1.21	1.31	7.34	1.28	0.0360	144	0.09	0.8352[e]	... [e]	3.92	5400	9
XO-3 b	1.21	1.37	11.8	1.22	0.0454	46	0.04	... [e]	... [e]	8.00	1700	10
HAT-P-11b	0.81	0.75	0.081	0.42	0.0530	0.2	0.01	... [e]	... [e]	29.2	0.1	11
CoRoT-7b	0.91	1.02	0.028	0.16	0.0170	8	0.29	... [e]	... [e]	16.8	80	12

References. — (1) Hebb et al. (2009) (2) Bean (2009) (3) Barge et al. (2008) (4) Winn et al. (2009a) (5) Sozzetti et al. (2009) (6) Pont et al. (2007b) (7) Pál et al. (2009) (8) Holman et al. (2007) (9) Joshi et al. (2009) (10) Johns-Krull et al. (2008) (11) Bakos et al. (2009) (12) `www.exoplanet.eu`[f]

Note. — These system parameters were used to estimate the detectability of apsidal precession for these very hot Jupiter systems. The derivation of the values in the remaining columns is described in the text and in the footnotes below. For all systems, $k_{2*} = 0.03$ and quadratic limb darkening parameters $u_1 = 0.35$ and $u_2 = 0.4$ (appropriate for *Kepler*'s bandpass) were used (Mandel & Agol, 2002). For reference, the measured eccentricity of WASP-12b, WASP-14b, HAT-P-11b, and XO-3b are 0.049 ± 0.015, 0.091 ± 0.003, 0.198 ± 0.046, and 0.2884 ± 0.0035 respectively. Other planets have unmeasured eccentricities or eccentricity upper limits of $\lesssim$0.05. A discussion of these results is provided in Section 2.3.4.

[a]We use $R_J \equiv 71492$ km, the equatorial radius at 1 bar.

[b]The estimated depth of the secondary transit in *Kepler*'s bandpass (see Section 2.3.1).

[c]The eccentricity required (at two different values of ω) so that a k_{2p} difference of 0.1 has an effective signal-to-noise of 1 in all of *Kepler* data for a V=14 star, corresponding to a photometric accuracy of 1000 ppm/min. If analogs to these planets were found by *Kepler* with the given eccentricities, the internal density distribution would be measured well enough to detect the presence of a large core (see Section 2.3.2). These values correspond to the circles in Figure 2.6. These results are for central transits (for $b > 0$, see Figure 2.7).

[d]The value of the change in period, $\dot{P}$, that can be detected with a signal-to-noise of 1 in all of *Kepler* data for a V=14 star (see Section 2.4.2). The value of threshold Q_* is an estimate of the maximum value of the stellar tidal dissipation parameter, Q_*, assuming that the period decay is due entirely to tidal evolution of the planet. Lower values of Q_* are detectable by *Kepler*. Stars are thought to have time-averaged Q_* values around 10000, though this value is highly uncertain and could be much higher for individual stars.

[e]Even with the precision of *Kepler*, apsidal precession for these planets is undetectable. The extrapolation used to compute eccentricities at specific values of threshold k_{2p} assumes the inverse relationship discussed in the text $k_{2p} \propto e^{-1}$, which is only true for low eccentricities.

[f]This ultra-short period low-mass planet was recently announced by the CoRoT team, but has not been published in a peer-reviewed journal. We take the parameters from J. Schneider's Extra-solar Planets Encyclopedia and use the mass-radius relation for terrestrial super-Earths of Sotin et al. (2007) to estimate the mass as ∼9 Earth masses (rather than using the quoted upper limit of 17 Earth masses).

sometimes extrapolated) our calculations to determine the eccentricity required to reach threshold k_{2p} values of 0.3, 0.1, and 0.01. These results are summarized in Figure 2.6 and Table 1.

WASP-12b is the best candidate for observing apsidal precession. With an eccentricity of $e \simeq 0.00026$ and k_{2p}=0.3, the apsidal precession would have an effective signal-to-noise of $\sim$1 for all of *Kepler* data. If e is $\sim$0.001, then k_{2p} can be well characterized and not just detected. As the difference in k_2 between Jupiter and Saturn of ~ 0.15 is primarily due to the presence of a massive core, a resolution in k_{2p} of 0.1 is enough to detect whether or not the planet has a core, at the $\sim$1-sigma level.

Although WASP-12b does not lie in the *Kepler* field, it clearly stands out as an excellent candidate for observing apsidal precession. Though the putative eccentricity of 0.049 (Hebb et al., 2009) is probably an overestimate (Laughlin et al., 2005), if it were real, it would cause sinusoidal transit timing deviations with an amplitude of $\sim$25 minutes (using Equation 2.20) and a period of $\sim$18 years. Such a large deviation would be readily observed from the ground in either transit times or transit shapes. If apsidal precession is not observed, tight upper limits on the eccentricity can be established.

Analogs to the very hot Jupiters WASP-4b, TrES-3b, CoRoT-1b, and OGLE-TR-56b are good candidates for observing apsidal precession if the eccentricities are above $\sim$0.003. (Note that CoRoT-1b has only $\sim$30 days of observations from the *CoRoT* satellite (Barge et al., 2008), which is insufficient to observe any of the effects discussed in this paper.) These planets have precession periods of around 100 years so that the argument of periapse of these planets changes by $\sim 10^\circ$ during the course of *Kepler* observations. Though none of these planets lie in the *Kepler* field, they are all good candidates for observing apsidal precession though precision photometry.

WASP-14b is more massive and has a larger semi-major axis (0.035 instead of 0.025) which is enough to significantly reduce the detectability of apsidal precession which only proceeds at 0.1° per year. Unlike the previously mentioned planets, WASP-14b has a known non-zero eccentricity of 0.091 ± 0.003 (Joshi et al., 2009). Thus, the amplitude of transit timing variations is known to be very large ($\sim$97 minutes), but with a $\sim$3400 year precession period.

CoRoT-7b is a very hot super-Earth and has the shortest known orbital period (excepting the ultra-short period planets of Sahu et al. 2006). We included this planet in our analysis to get a feel for the plausibility of detecting the interior structure of terrestrial extra-solar planets. The small radius reduces the planetary contribution to apsidal precession (Figure 1) and significantly reduces the photometric signal. We note here that in bodies where material strength (rigidity) is more important than self-gravity, k_{2p} is no longer directly related to internal density distribution. The correction factor is typically small for bodies larger than the Earth (Murray & Dermott, 1999).

XO-3b is a super-massive eccentric planet that is not in the *Kepler* field. Even so, it is interesting to note that, using the known eccentricity $e = 0.2884 \pm 0.0035$ (Winn et al., 2009b) and accounting

for the brightness of the host star (V=9.8), the *Kepler* threshold k_{2p} is reduced to only 0.54. As pointed out by Jordan & Bakos (2008) and Pál & Kocsis (2008), XO-3b is a good candidate for observing apsidal precession within the next decade or so. Furthermore, as discussed below, the non-zero obliquity of the stellar spin axis (Winn et al., 2009b) may also result in an observable signal due to nodal precession.

HAT-P-7b and HAT-P-11b are orbiting bright stars in the *Kepler* field. The latter is an eccentric hot Neptune with a relatively large semi-major axis resulting in no eminently detectable apsidal precession. HAT-P-7b, on the other hand, is a good candidate for detecting apsidal precession. It is probably one of the brightest hot Jupiters in the *Kepler* field, orbiting a V=10.5 star. The system brightness improves the expected photometric accuracy from 1000 ppm/min to 200 ppm/min, implying that an eccentricity of only 0.014 is needed to detect apsidal precession (threshold k_{2p}=0.3). Pál et al. (2009) report a best-fit eccentricity of 0.003 ± 0.012, indicating that the necessary eccentricity cannot be ruled out. Furthermore, this planet has transiting data extending back to 2004 and was observed by NASA's *EPOXI* Mission in 2008 (Christiansen et al., 2009; D. Deming, pers. comm.). This additional baseline, though sparsely sampled, may provide the additional leverage needed to detect apsidal precession if the eccentricity is non-zero. Note, however, that detecting changes in transit shapes is more difficult when the observations are made with a variety of telescopes because transit shapes depend on the observing filter used, due to wavelength-dependent limb darkening.

TrES-2b is similar to HAT-P-7b in that it also lies in the *Kepler* field, has observations dating to 2005, and was observed by NASA's *EPOXI* Mission. TrES-2b is somewhat fainter than HAT-P-7b (V=11.4), and, correcting for the system brightness, an eccentricity of 0.021 would result in detectable apsidal precession (threshold k_{2p}=0.3). Observations of the secondary eclipse show no detectable deviations of the orbit from circularity (O'Donovan et al., 2009). Even so, the light curve of this planet is quite sensitive to perturbations as it has a quite high impact parameter $b = 0.854$. Accounting for this impact parameter does not significantly change the required eccentricity.

We conclude that *Kepler may detect the cores of very hot Jupiters* and probe their interior structure though their evolving transit light curve if eccentricities are above $\sim$0.003. As future observations provide longer baselines for these observations, the sensitivity to interior structure measurements will increase dramatically, significantly lowering the eccentricity needed to observe apsidal precession.

In cases where apsidal precession is not observed, the data can set strong upper limits on planetary eccentricities. An upper limit on the eccentricity can be inferred by assuming that the planet has the minimal physically-plausible value of $k_{2p} \approx 0.1$. Null detections of apsidal motion should therefore provide upper limits on eccentricity comparable to the values shown in Table 1 (also shown by circles in Figure 2.6). Such strong eccentricity constraints are valuable for improving our understanding of these close-in planets.

2.4 Potential Confusion of the Apsidal Precession Signal

In the above, we have assumed that measuring $\dot{\omega}$ is tantamount to measuring k_{2p}. This is justified by noting that the conversion $\dot{\omega}$ to k_{2p} involves only factors that are very well characterized. In Section 2 and Figure 1, we showed that k_{2p} is usually the dominant source of apsidal precession. The effects of k_{2*} and general relativity are well-understood and can typically be subtracted away without introducing serious uncertainty, even when they dominate the apsidal precession rate. From Equation 2.6, converting the remaining $\dot{\omega}_{\rm p}$ to k_{2p} requires only knowing $\frac{M_p}{M_*}$, e, $\frac{R_p}{a}$, and n. The latter two are very accurately measured with even a few transit light curves (e.g., Torres et al., 2008; Southworth, 2008). The eccentricity only enters the equation through the $f_2(e)$ and $g_2(e)$ eccentricity functions (Equations 2.7 and 2.11), and *Kepler* observations of secondary eclipse are sufficiently accurate to remove any systematic error due to these terms unless the eccentricity is large ($e \gtrsim 0.3$). Determining the mass ratio requires well-sampled radial velocity observations. The systems detected by *Kepler* are bright enough to get good mass measurements, especially since very hot Jupiters have large radial velocity amplitudes ($K \sim 200$ m/s).[8] The anticipated error in the mass ratio is a few percent (Torres et al., 2008). In all, we estimate that, converting from $\dot{\omega}$ to k_{2p} leads to a typical systematic error on k_{2p} of around $\sim$.01. This is a relatively small systematic effect in comparison to the potential range ($\sim$0.5) of k_{2p} values. For reference, the eccentricity required to reach a threshold k_{2p} of 0.01 is shown in Figure 2.6 by squares.

Another way to introduce systematic errors on the measurement of k_{2p} is to misinterpret similar transit light curve variations. To ensure that the method outlined in this paper truly probes the interiors of extra-solar planets, we consider in this section whether the transit light curve resulting from apsidal precession can be confused with any other common circumstances. Although a very specific combination of parameters is required for any particular phenomenon to successfully mimic a signal due to k_{2p}, the below effects should be reconsidered when actual data is available.

2.4.1 Testing the Effect of Obliquity

If either the star or planet has a non-zero obliquity, the orbital plane will no longer be fixed as a result of nodal precession. The obliquities of very hot Jupiters rapidly ($\lesssim$ 1 MYr) decay to a Cassini state, and recent work has shown that these planets are likely in Cassini state 1 (Winn & Holman, 2005; Levrard et al., 2007; Fabrycky et al., 2007). Using a model based on the equations of Eggleton & Kiseleva-Eggleton (2001), we found that Cassini obliquities of very hot Jupiters are indeed negligible ($\alpha_p < 0.01^\circ$). Though tidal damping of the stellar obliquity occurs on far longer timescales, several measurements of the projected stellar obliquity through the Rossiter-McLaughlin

[8] Other than determining the mass ratio and constraining the eccentricity, radial velocity information is thought to have a negligible contribution in constraining apsidal precession unless a serious observational campaign can measure the radial velocity period (independently of transits) to sub-second accuracies. (Heyl & Gladman, 2007; Jordan & Bakos, 2008).

effect indicates that planet-hosting stars generally have low obliquities $\lesssim 10^\circ$ like the Sun (Fabrycky & Winn, 2009). Hence, the general expectation is that both the star and planet will have rather low, but potentially non-zero obliquities.

Understanding the specific orbital evolution resulting from non-zero obliquities is more complicated than the simple prescription for apsidal precession. To correctly account for non-Keplerian effects, we wrote a direct integrator, following Mardling & Lin (2002), that calculates the Cartesian trajectory (and the direction of the spin axes) of a star-planet system including general relativity and the effects of quadrupolar distortion. This integrator reproduces the orbit-averaged analytic equations of Mardling & Lin (2002), which are the same as those in Eggleton & Kiseleva-Eggleton (2001), Sterne (1939a), and elsewhere.[9] We did not include the effects of tidal forces or additional planets which are not relevant to our problem.

Using this direct integrator, we investigated the effect of non-zero obliquities on the transit times, durations, and impact parameters. Integration of several cases with varying stellar and planetary obliquities showed that the largest effect on the photometry was due to changes in the impact parameter, as expected for an orbit with changing orientation (Miralda-Escudé, 2002). However, even for large stellar obliquities ($\sim 45^\circ$) the transit light curve variations due to obliquity are generally small relative to the effects of purely apsidal precession, even with low eccentricities. One reason for this is that the tidal bulge, which does not contribute to nodal precession, is $\gtrsim 15$ times more important than the rotational bulge. As with apsidal precession, the planetary contribution to orbital variations is much stronger than the stellar contribution (for equal obliquities). Unless the planetary obliquity is unexpectedly large ($\gtrsim 0.5^\circ$), the obliquity-induced nodal precession should have only a minor effect on the transit light curve.

2.4.2 Transit Timing due to Orbital Decay

Orbital decay generates a small secular trend in transit times. Sasselov (2003) proposed the detectability of the expected $\sim$1 ms/yr period change due to semi-major axis decay of OGLE-TR-56b. The transit timing anomaly due solely to orbital decay (or growth) is the result of constantly accumulating changes in the period:

$$T_N \simeq T_0 + NP_{\rm obs} + \frac{1}{2}N^2\delta P \tag{2.23}$$

where $\delta P \equiv \dot{P}P$ is the change in the period during one orbit and N is the number of transits after the initial transit. Equation 2.23 can be derived by noting that the transit times are basically the integral of the instantaneous period. As before, the transit timing anomaly is composed of the

[9]This involved minor modifications to the "direct integrator" equations 3 and 5 in Mardling & Lin (2002). In Equation 3, the coefficient 12 should be a 6 (R. Mardling, pers. comm.) and Equation 5 was replaced with the nearly equivalent equation from Soffel (1989).

quadratic deviation of T_N from a straight line. The change in period can be due to magnetic stellar breaking (e.g., Lee et al., 2009; Barker & Ogilvie, 2009a), the Yarkovsky effect applied to planets (Fabrycky, 2008a), and/or other effects.

For planets orbiting an asynchronously rotating star, a major source of orbital decay is tidal evolution, which results in a slow change in semi-major axis, according to the formula (Murray & Dermott, 1999):

$$\dot{a} = \text{sign}(\nu_* - n)\frac{3k_{2*}}{Q_*}\frac{M_p}{M_*}\left(\frac{R_*}{a}\right)^5 na \tag{2.24}$$

where sign(x) returns the sign of x or 0 if $x = 0$ and where Q_* is the tidal quality parameter of the star, typically around 10^4 (Dobbs-Dixon et al., 2004). Though δP due to tidal dissipation is only of order 3 micro-seconds, N grows by ~ 300 each year, reaching $\sim$1000 during the duration of *Kepler* for very hot Jupiters. This implies a transit timing signal of about a few seconds.

Calculating the total "signal-to-noise" of tidal evolution, as was done for k_{2p}, we find that reasonable values of Q_* can be measured even for faint stars ($V = 14$; 1000 ppm/min noise). For a circular orbit with the parameters of OGLE-TR-56b, the effective $\frac{S}{N}$ reaches 1 when $\dot{P}$ is 1.36 ms/yr (see Table 1), corresponding to $Q_* \approx 25000$. This implies the detectability of most of the empirically-motivated estimates of Sasselov (2003) for the tidal decay of OGLE-TR-56b, which are estimated to be within an order of magnitude of 1 ms/yr. On the other hand, Barker & Ogilvie (2009b) estimate that the tidal damping in F-stars like OGLE-TR-56 and WASP-12 may be very low, which may explain the survival of these short period planets.

The estimates of the threshold values of $\dot{P}$, shown in Table 1, include removing degeneracies in other parameters, except apsidal precession of eccentric orbits, and assume that everything but $\dot{P}$ is known. Note that the transit light curve signal due to orbital decay is due entirely to transit timing; the change in a is far too small to observe in transit shaping. As the signal due to apsidal precession includes significant changes to the shapes of the transits, the signal due to k_{2p} is qualitatively different than that of Q_*. The shifting of secondary transits from precession also help in this regard, as outlined above. However, the primary transit timing signals can be similar: quadratic transit timing anomalies with amplitudes of $\sim$1 second.

Kepler analogs of very hot Jupiters WASP-12b, OGLE-TR-56b, CoRoT-1b, WASP-4b, and TrES-3b could have detectable transit timing anomalies due to tidal decay, implying a direct measurement of the current value of Q_* for specific stars (Table 1). This is an exciting possibility, providing the first direct measurements (or constraints) of the currently unknown details of tidal dissipation in a variety of individual stars.[10] We also note that interesting orbital decay of eclipsing binary systems seen by *Kepler* could also be detectable.

[10]The vanishingly small effect of eccentricity decay is $\sim \frac{1}{Q_p}$ smaller than apsidal precession, so that direct measurements of Q_p from eccentricity decay are not feasible.

2.4.3 Confusion Due to Other Planets

Could the signal due to k_{2p} be confused with additional planets? In considering this issue, it should be noted that all known hot Jupiters (with $a \lesssim 0.05$ AU and $M_p \gtrsim 0.5 M_{Jup}$) have no currently known additional companions. The apparent single nature of these systems could very well be due to observational biases (Fabrycky, 2008b). However, even for stars that have been observed for many years with radial velocity (e.g., 51 Peg, HD 209458), there appears to be a strong tendency towards hot Jupiters as the only close-in massive planets.

Previous studies of transit timing variations focus on the effects of additional planetary perturbers (e.g., Holman & Murray, 2005; Agol et al., 2005; Ford & Holman, 2007; Nesvorný & Morbidelli, 2008). These authors find that nearby massive planets or even low-mass planets in mean-motion resonances would cause strong transit timing variations that are easily distinguishable from the comparatively long-period timing anomalies due to k_{2p}. Relatively distant companions or non-resonant low-mass planets, however, can induce a linear apsidal precession signal just like k_{2p} (Miralda-Escudé, 2002; Heyl & Gladman, 2007; Jordan & Bakos, 2008). The precession rate induced by a perturbing body is a function of its mass and semi-major axis. The interior structure of very hot Jupiters causes apsidal precession as fast as a few degrees per year. To match this precession rate would require, for example, another Jupiter-mass planet at $\lesssim 0.1$AU or a solar-mass star at $\sim$1 AU. Even perturbers an order of magnitude smaller than these would be readily detectable using radial velocity observations and/or high-frequency transit time variations. When restricted to planets that are undetectable by other means, adding the precession due to the unknown perturbing planet would lead to an insignificant overestimate of k_{2p} for very hot Jupiters.[11] When observing transiting planets with larger semi-major axes ($a \gtrsim 0.05$ AU), the strength of planetary induced apsidal precession is reduced to a level comparable to apsidal precession from a low-mass perturbing planet (Jordan & Bakos, 2008) and confusion may be possible in these cases.

Since the transit timing signal for apsidal precession is similar to a sinusoid, another potential source of confusion would be light-travel time offsets due to a distant orbiting companion (e.g., Deeg et al., 2008). The transit timing signal due to stellar motion about the barycenter can be distinguished from k_{2p} precession[12] by considering the changes in transit shapes and primary-secondary transit time offsets, which are not affected by distant companions.

We conclude that transit timing effects from other planets can be readily distinguished from the effects of apsidal precession. To address the issue of the transit shaping signal due to additional planets, we wrote a simple three-body integrator (similar to the integrator mentioned above) to investigate the kinds of transit light curve signals created by additional planets. For the vast majority

[11] Conversely, as a consequence of the fast precession of very hot Jupiters due to their (unknown) interiors, it will be very difficult to detect the presence of additional perturbing planets in these systems from apsidal precession alone.

[12] Transit time anomalies due to Q_* (Section 2.4.2), however, can be confused with barycenter light-travel time shifts due to a distant planet that may be undetectable in radial velocities.

of additional planet parameters, the transit timing deviations always carry far more signal than the minor deviations due to changes in the angular velocity[13] ($\dot{f}_{tr}$) or impact parameter (b), which together determine the transit shape as described in Section 2.3.3 above. Generally, it is much easier to delay a transit by 5 seconds than it is to shift the apparent transit plane by an appreciable amount.

However, when the perturbing planet is on a plane highly-inclined to the transiting planet, changes in the transit shape can become detectable, even while the transit timing variations are negligible. For example, a perturbing planet of mass $10^{-5}M_*$ at 0.1 AU with a mutual inclination of 45° caused very hot Jupiter transit durations to change by ∼1 second/year. This kind of signal is the result of nodal precession induced by the perturbing planet, as originally pointed out by Miralda-Escudé (2002). In our investigation, we found that the three-body nodal precession alters the impact parameter (b) but does not significantly affect the orbital angular velocity ($\dot{f}_{tr}$). Conversely, the transit shaping signal due to k_{2p} is generally produced by changes in both b and $\dot{f}_{tr}$, but at near-central transits, the effect of changing orbital velocity is dominant (see Section 2.3.3). In high-precision transit light curves, both the angular velocity and the impact parameter can be independently measured and hence the signals of apsidal and nodal precession are usually distinct for all but the most grazing transits.

Given the uniqueness of the apsidal precession signal induced by the planet's interior, it appears that if additional planets are not detectable in radial velocities, transit timing variations, or nodal precession, then they will not contribute to a misinterpretation of an inferred value of k_{2p} for very hot Jupiters. Nevertheless, future measurements of k_{2p} should check that these issues are unimportant within the context of the specific system being studied.

Finally, we estimate that moons or rings with enough mass to bias an inferred k_{2p} would cause other readily detectable photometric anomalies (e.g., planet-moon barycentric motion Sartoretti & Schneider, 1999). In addition, extra-solar moons with any significant mass are tidally unstable, especially around very hot Jupiters (Barnes & O'Brien, 2002).

2.5 Other Methods for Determining k_{2p}

2.5.1 Secular Evolution of a Two Planet System

Measuring k_2 for an extra-solar planet was suggested by Wu & Goldreich (2002) for the inner planet of HD 83443. Unfortunately, later analyses have indicated that the supposed second planet in this system was actually an artefact of the sparse radial velocity data (Mayor et al., 2004). Nevertheless, this technique could be applied to other eccentric planetary systems with similar

[13]The angular velocity is directly related to the star-planet separation through conservation of angular momentum: $r\dot{f}^2$.

conditions (Mardling, 2007). Wu & Goldreich (2002) showed that in a regime of significant tidal circularization and excitation from an additional planet, the ratio of eccentricities depends on the precession rate which is dominated by k_{2p} as shown above (see also Adams & Laughlin 2006, who do not include precession due to the planetary quadrupole). In theory, the current orbital state of such multi-planet systems gives an indirect measurement of the apsidal precession rate.

2.5.2 Direct Detection of Planetary Asphericity

Another method for determining interior properties of transiting planets would be to directly measure the asphericity due to the rotational or tidal bulge in primary transit photometry. The height of the rotational and tidal bulges are $q_r h_2 R_p$ and $q_t h_2 R_p$, respectively, where q_r and q_t are the dimensionless small parameters defined in Equation 2.2 and h_2 is another Love number which, for fluid bodies, is simply $k_2 + 1$ (Sterne, 1939a). These bulges cause the disk of the planet to be slightly elliptical, subtly modifying the photometric signal, as discussed for rotational bulges by Seager & Hui (2002) and Barnes & Fortney (2003). However, as discussed by Barnes & Fortney (2003), in real systems with actual observations, the size of the rotational bulge is very difficult to determine as it is highly correlated with stellar and orbital parameters that are not known *a priori*, e.g., limb darkening coefficients.

The tidal bulge, whose height is also set by k_{2p}, does not suffer from some of the difficulties involved with measuring the rotational bulge. It has a known orientation (pointing towards the star) so there is no degeneracy from an unknown obliquity (Barnes & Fortney, 2003). (Note, however, that for hot Jupiters, the obliquities must be tidally evolved to nearly zero, so this isn't really a problem with the rotational bulge.) In addition, the signal due to oblateness is only significant near ingress/egress, but the tidal bulge is continuously changing orientation throughout the entire transit. Though the tidal bulge is typically three times larger than the rotational bulge (Equation 2), the projection of the tidal bulge that is seen during a transit is small, proportional to $\sin\theta$ where θ is the angle between the planet position and the Earth's line of sight. For very hot Jupiters that have semi-major axes of only $\lesssim$6 stellar radii, $\sin\theta$ during transit ingress/egress reaches $\gtrsim \frac{1}{6}$ so that the projected tidal bulge is about half as large as the rotational bulge. The extra dimming due to the tidal bulges (and rotational bulges) is as high as 2×10^{-4} for some planets that are expected to have tides over 2000 km high (e.g., WASP-12b, WASP-4b, Corot-1b, OGLE-TR-56b); this compares very favorably with the photometric accuracy of binned *Kepler* data at about 10 ppm per minute. However, we expect that, as with the rotational bulge alone, the combined signal from the rotational and tidal bulge will be highly degenerate with the unknown limb-darkening coefficients, as the size of the projection of the tidal bulge also varies as the distance to the center of the star.

We note that using multi-color photometry should significantly improve the prospects of detecting non-spherical planetary transits since it breaks most of these degeneracies. For example, Knutson

et al. (2007b) use HST to observe transits of HD 209458b in 10 wavelength bands and measure the planetary radius with a relative accuracy (between bands) of $0.003R_J$, of the same level as the change in shape due to oblateness and the tidal bulge. Pont et al. (2007a) made a similar measurement for HD 189733b and reached even higher relative accuracy. Combining such measurements with other data (e.g., primary transits in the infrared, where limb-darkening is much smaller) and a stellar photosphere model (to correctly correlate limb darkening parameters as in Agol & Steffen 2007) could yield detections of planetary asphericity, especially in very hot Jupiters which have the largest bulges.

One possible source of confusion in interpreting planetary asphericity is the thermally-induced pressure effects of an unevenly radiated surface. In non-synchronous planets, the thermal tidal bulge (Arras & Socrates, 2009) can shift the level of the photosphere by approximately an atmospheric scale height, about 10^{-2} or 10^{-3} planetary radii (P. Arras, pers. comm.). The orientation of the thermal bulge is significantly different from the tidal or rotational bulges and should be distinguishable. Furthermore, very hot Jupiters should orbit synchronously, reducing the importance of this effect. Nevertheless, the effect of atmospheric phenomena on measurements of planetary asphericity should be considered.

Though difficult to disentangle from other small photometric effects, high-precision multi-color photometry may be another viable method for measuring k_{2p}. This technique is complimentary to detecting k_{2p} from apsidal precession since it does not require that the planet is eccentric, nor does it require a long time baseline. On some planets, the two methods could be used together as mutual confirmation of the planetary interior structure.

2.6 Conclusions

The planetary mass and radius are the only bulk physical characteristics measured for extra-solar planets to date. In this paper, we find that the planetary Love number (k_{2p}, equivalent to J_2) can also have an observationally detectable signal (quadrupole-induced apsidal precession) which can provide a new and unique probe into the interiors of very hot Jupiters. In particular, k_{2p} is influenced by the size of a solid core and other internal properties. Core sizes can be used to infer the formation and evolution of individual extra-solar planets (e.g., Dodson-Robinson & Bodenheimer, 2009; Helled & Schubert, 2009).

The presence of a nearby massive star creates a large tidal potential on these planets, raising significant tidal bulges which then induce non-Keplerian effects on the star-planet orbit itself. The resulting apsidal precession accounts for $\sim$95% of the total apsidal precession in the best cases (Figure 2.1). Hence, we find that the internal density distribution, characterized by k_{2p}, has a large and clear signal, not to be confused with any other parameters or phenomena. We urge those

modeling the interior structures of extra-solar planets to tabulate the values of k_{2p} for their various models.

Encouraged by this result, we calculated full photometric light-curves like those expected from the *Kepler* mission to determine the realistic observability of the interior signal. We estimate that *Kepler* should be able to distinguish between interiors with and without massive cores ($\Delta k_{2p} \simeq 0.1$) for very hot Jupiters with eccentricities around $e \sim 0.003$ (Figure 2.6). Eccentricities this high may occur for some of the very hot Jupiters expected to be found by *Kepler*, though these planets usually have highly damped eccentricities. Much stronger constraints on apsidal precession can be obtained by combining *Kepler* photometry with precise secondary transits observed in the infrared. In cases where apsidal precession is not observed, the data can set strong upper limits on planetary eccentricities.

In analyzing *Kepler*'s photometric signal of apsidal precession, we find that transit timing variations are an almost negligible source of signal, though transit timing has been the focus of many observational and theoretical papers to date. The effect of "transit shaping" has ∼30 times the photometric signal of transit timing for apsidal precession (see Figure 2.3, Pál & Kocsis, 2008; Jordan & Bakos, 2008)). At orientations where transit timing and shaping are weakest, the changing offset between primary and secondary transit times can be used to measure k_{2p} (Figure 2.4). It may also be possible to measure k_{2p} from high-precision multi-color photometry by directly detecting the planetary asphericity in transit. Such a measurement does not require a long baseline or an eccentric orbit.

Very hot Jupiters are also excellent candidates for detecting tidal semi-major axis decay, where we find that relatively small period changes of $\dot{P} \simeq 1$ ms/yr should be detectable. This could constitute the first measurements (or constraints) on tidal Q_* for a variety of individual stars. We note that *Kepler* measurements of transit timing and shaping for eclipsing binaries should also provide powerful constraints on stellar interiors through apsidal motion and binary orbital decay (due to tides, if the components are asynchronous).

Accurately measuring the interior structure of distant extra-solar planets seems too good to be true. Nevertheless, the exquisite precision, constant monitoring, and 3.5-year baseline of the *Kepler* mission combined with the high sensitivity of transit light curves to small changes in the star-planet orbit make this measurement plausible.

Our focus on *Kepler* data should not be interpreted to mean that other observations will be incapable of measuring k_{2p}. In fact, the opposite is true since the size of the apsidal precession signal increases dramatically with a longer baseline. Combining *Kepler* measurements with future ground and space based observations can create a powerful tool for measuring k_{2p}. In the far future, many planets will have measured apsidal precession rates (like eclipsing binary systems have now) and inferred k_{2p} values. Incorporating these measurements into interior models holds promise for

greater understanding of all extra-solar planets.

Acknowledgments: We thank Dave Stevenson, Mike Brown, Greg Laughlin, Oded Aharonson, Thomas Beatty, Phil Arras, Rosemary Mardling, Re'em Sari, Alejandro Soto, Ian McEwen and Chris Lee for help and useful discussions. We especially thank the referee, Dan Fabrycky, for helpful suggestions and discussions. DR is grateful for the support of the Moore Foundation. ASW is grateful for support from the National Science Foundation. This research has made use of NASA's Astrophysics Data System.

Bibliography

Adams, F. C., & Laughlin, G. 2006, Astrophysical Journal, 649, 1004, arXiv:astro-ph/0606349

Agol, E., Cowan, N. B., Bushong, J., Knutson, H., Charbonneau, D., Deming, D., & Steffen, J. H. 2009, in IAU Symposium, Vol. 253, IAU Symposium, 209–215

Agol, E., Steffen, J., Sari, R., & Clarkson, W. 2005, Monthly Notices of the RAS, 359, 567, arXiv:astro-ph/0412032

Agol, E., & Steffen, J. H. 2007, Monthly Notices of the RAS, 374, 941, arXiv:astro-ph/0610159

Alonso, R., Aigrain, S., Pont, F., Mazeh, T., & The CoRoT Exoplanet Science Team. 2009, in IAU Symposium, Vol. 253, IAU Symposium, 91–96

Arras, P., & Socrates, A. 2009, ArXiv e-prints, 0901.0735

Bakos, G. Á. et al. 2009, ArXiv e-prints, 0901.0282

Baraffe, I., Chabrier, G., & Barman, T. 2008, 0802.1810

Barge, P. et al. 2008, 0803.3202

Barker, A. J., & Ogilvie, G. I. 2009a, ArXiv e-prints, 0902.4554

——. 2009b, ArXiv e-prints, 0902.4563

Barnes, J. W., & Fortney, J. J. 2003, Astrophysical Journal, 588, 545, arXiv:astro-ph/0301156

Barnes, J. W., & O'Brien, D. P. 2002, Astrophysical Journal, 575, 1087, arXiv:astro-ph/0205035

Batten, A. H. 1973, Binary and multiple systems of stars (Binary and multiple systems of stars / by Alan H. Batten. Oxford ; New York : Pergamon Press, [1973] (International series of monographs in natural philosophy ; v. 51))

Bean, J. L. 2009, ArXiv e-prints, 0903.1845

Beatty, T. G., & Gaudi, B. S. 2008, ArXiv e-prints, 804, 0804.1150

Bodenheimer, P., Lin, D. N. C., & Mardling, R. A. 2001, Astrophysical Journal, 548, 466

Borucki, W. J. et al. 2003, in Presented at the Society of Photo-Optical Instrumentation Engineers (SPIE) Conference, Vol. 4854, Future EUV/UV and Visible Space Astrophysics Missions and Instrumentation. Edited by J. Chris Blades, Oswald H. W. Siegmund. Proceedings of the SPIE, Volume 4854, pp. 129-140 (2003)., ed. J. C. Blades & O. H. W. Siegmund, 129–140

Burrows, A., Hubeny, I., Budaj, J., & Hubbard, W. B. 2007, Astrophysical Journal, 661, 502, arXiv:astro-ph/0612703

Burrows, A., Ibgui, L., & Hubeny, I. 2008, ArXiv e-prints, 803, 0803.2523

Charbonneau, D. 2003, in Astronomical Society of the Pacific Conference Series, Vol. 294, Scientific Frontiers in Research on Extrasolar Planets, ed. D. Deming & S. Seager, 449–456

Charbonneau, D. et al. 2005, Astrophysical Journal, 626, 523, arXiv:astro-ph/0503457

Charbonneau, D., Brown, T. M., Latham, D. W., & Mayor, M. 2000, Astrophysical Journal, Letters, 529, L45, arXiv:astro-ph/9911436

Chatterjee, S., Ford, E. B., & Rasio, F. A. 2007, ArXiv Astrophysics e-prints, astro-ph/0703166

Christian, D. J. et al. 2008, ArXiv e-prints, 806, 0806.1482

Christiansen, J. L. et al. 2009, in IAU Symposium, Vol. 253, IAU Symposium, 301–307

Claret, A. 1995, Astronomy and Astrophysics, Supplement, 109, 441

Cowling, T. G. 1938, Monthly Notices of the RAS, 98, 734

Deeg, H. J., Ocaña, B., Kozhevnikov, V. P., Charbonneau, D., O'Donovan, F. T., & Doyle, L. R. 2008, Astronomy and Astrophysics, 480, 563, arXiv:0801.2186

Dobbs-Dixon, I., Lin, D. N. C., & Mardling, R. A. 2004, Astrophysical Journal, 610, 464, arXiv:astro-ph/0408191

Dodson-Robinson, S. E., & Bodenheimer, P. 2009, ArXiv e-prints, 0901.0582

Eggleton, P. P., & Kiseleva-Eggleton, L. 2001, Astrophysical Journal, 562, 1012, arXiv:astro-ph/0104126

Fabrycky, D. 2008a, Astrophysical Journal, Letters, 677, L117, 0803.1839

Fabrycky, D., & Tremaine, S. 2007, Astrophysical Journal, 669, 1298, arXiv:0705.4285

Fabrycky, D. C. 2008b, ArXiv e-prints, 806, 0806.4314

Fabrycky, D. C., Johnson, E. T., & Goodman, J. 2007, Astrophysical Journal, 665, 754, arXiv:astro-ph/0703418

Fabrycky, D. C., & Winn, J. N. 2009, ArXiv e-prints, 0902.0737

Ferraz-Mello, S., Rodríguez, A., & Hussmann, H. 2008, 0712.1156

Ford, E. B., & Holman, M. J. 2007, Astrophysical Journal, Letters, 664, L51, arXiv:0705.0356

Ford, E. B., Lystad, V., & Rasio, F. A. 2005, Nature, 434, 873, arXiv:astro-ph/0502441

Gillon, M., Anderson, D. R., Demory, B. ., Wilson, D. M., Hellier, C., Queloz, D., & Waelkens, C. 2008, ArXiv e-prints, 806, 0806.4911

Goldreich, P., & Soter, S. 1966, Icarus, 5, 375

Gomes, R., Levison, H. F., Tsiganis, K., & Morbidelli, A. 2005, Nature, 435, 466

Goodman, J. 2009, ArXiv e-prints, 0901.3279

Gu, P.-G., & Ogilvie, G. I. 2009, ArXiv e-prints, 0901.3401

Guillot, T. 2005, Annual Review of Earth and Planetary Sciences, 33, 493, arXiv:astro-ph/0502068

Guillot, T., Santos, N. C., Pont, F., Iro, N., Melo, C., & Ribas, I. 2006, Astronomy and Astrophysics, 453, L21, arXiv:astro-ph/0605751

Hebb, L. et al. 2009, Astrophysical Journal, 693, 1920, 0812.3240

Helled, R., & Schubert, G. 2009, ArXiv e-prints, 0903.1997

Heyl, J. S., & Gladman, B. J. 2007, Monthly Notices of the RAS, 377, 1511, arXiv:astro-ph/0610267

Holman, M. J., & Murray, N. W. 2005, Science, 307, 1288

Holman, M. J. et al. 2007, Astrophysical Journal, 664, 1185, 0704.2907

Hood, B., Wood, K., Seager, S., & Collier Cameron, A. 2008, ArXiv e-prints, 807, 0807.1561

Hut, P. 1981, Astronomy and Astrophysics, 99, 126

Iorio, L. 2006, New Astronomy, 11, 490, arXiv:gr-qc/0505107

Jackson, B., Greenberg, R., & Barnes, R. 2008, 0801.0716

Johns-Krull, C. M. et al. 2008, Astrophysical Journal, 677, 657, 0712.4283

Jordan, A., & Bakos, G. A. 2008, ArXiv e-prints, 806, 0806.0630

Joshi, Y. C. et al. 2009, Monthly Notices of the RAS, 392, 1532, 0806.1478

——. 2008, ArXiv e-prints, 806, 0806.1478

Kallrath, J., Milone, E. F., Kallrath, J., & Milone, E. F., eds. 1999, Eclipsing binary stars : modeling and analysis

Kjeldsen, H., Bedding, T. R., & Christensen-Dalsgaard, J. 2008, ArXiv e-prints, 807, 0807.0508

Knutson, H. A. et al. 2007a, Nature, 447, 183, arXiv:0705.0993

Knutson, H. A., Charbonneau, D., Noyes, R. W., Brown, T. M., & Gilliland, R. L. 2007b, Astrophysical Journal, 655, 564, arXiv:astro-ph/0603542

Koch, D. et al. 2006, Astrophysics and Space Science, 304, 391

Kopal, Z. 1959, Close binary systems (The International Astrophysics Series, London: Chapman & Hall, 1959)

Kopal, Z., ed. 1978, Astrophysics and Space Science Library, Vol. 68, Dynamics of Close Binary Systems

Kozai, Y. 1959, Astronomical Journal, 64, 367

Lanza, A. F. et al. 2009, Astronomy and Astrophysics, 493, 193, 0811.0461

Laughlin, G., Marcy, G. W., Vogt, S. S., Fischer, D. A., & Butler, R. P. 2005, Astrophysical Journal, Letters, 629, L121

Lee, J. W., Kim, S.-L., Kim, C.-H., Koch, R. H., Lee, C.-U., Kim, H.-I., & Park, J.-H. 2009, Astronomical Journal, 137, 3181, 0811.3807

Levrard, B., Correia, A. C. M., Chabrier, G., Baraffe, I., Selsis, F., & Laskar, J. 2007, Astronomy and Astrophysics, 462, L5, arXiv:astro-ph/0612044

Levrard, B., Winisdoerffer, C., & Chabrier, G. 2009, Astrophysical Journal, Letters, 692, L9, 0901.2048

Loeb, A. 2005, Astrophysical Journal, Letters, 623, L45, arXiv:astro-ph/0501548

——. 2008, ArXiv e-prints, 807, 0807.0835

López-Morales, M., & Seager, S. 2007, Astrophysical Journal, Letters, 667, L191, arXiv:0708.0822

Mandel, K., & Agol, E. 2002, Astrophysical Journal, Letters, 580, L171, arXiv:astro-ph/0210099

Mardling, R. A. 2007, Monthly Notices of the RAS, 382, 1768, arXiv:0706.0224

Mardling, R. A., & Lin, D. N. C. 2002, Astrophysical Journal, 573, 829

Matsumura, S., Takeda, G., & Rasio, F. A. 2008, Astrophysical Journal, Letters, 686, L29, 0808.3724

Mayor, M., Udry, S., Naef, D., Pepe, F., Queloz, D., Santos, N. C., & Burnet, M. 2004, Astronomy and Astrophysics, 415, 391, arXiv:astro-ph/0310316

Miralda-Escudé, J. 2002, Astrophysical Journal, 564, 1019, arXiv:astro-ph/0104034

Murray, C. D., & Dermott, S. F. 1999, Solar system dynamics (Solar system dynamics by Murray, C. D., 1999)

Nesvorný, D., & Morbidelli, A. 2008, Astrophysical Journal, 688, 636

O'Donovan, F. T., Charbonneau, D., Harrington, J., Seager, S., Deming, D., & Knutson, H. A. 2009, in IAU Symposium, Vol. 253, IAU Symposium, 536–539

Pál, A., Bakos, G. Á., Noyes, R. W., & Torres, G. 2009, in IAU Symposium, Vol. 253, IAU Symposium, 428–431

Pál, A., & Kocsis, B. 2008, ArXiv e-prints, 806, 0806.0629

Peale, S. J., Cassen, P., & Reynolds, R. T. 1979, Science, 203, 892

Pont, F. et al. 2007a, Astronomy and Astrophysics, 476, 1347, arXiv:0707.1940

——. 2007b, Astronomy and Astrophysics, 465, 1069, arXiv:astro-ph/0610827

Rafikov, R. R. 2008, ArXiv e-prints, 807, 0807.0008

Rodriguez, A., & Ferraz-Mello, S. 2009, ArXiv e-prints, 0903.0763

Rowe, J. F. et al. 2007, ArXiv e-prints, 711, 0711.4111

Russell, H. N. 1928, Monthly Notices of the RAS, 88, 641

Sahu, K. C. et al. 2006, Nature, 443, 534, arXiv:astro-ph/0610098

Sartoretti, P., & Schneider, J. 1999, Astronomy and Astrophysics, Supplement, 134, 553

Sasselov, D. D. 2003, Astrophysical Journal, 596, 1327, arXiv:astro-ph/0303403

Scharf, C. A. 2007, Astrophysical Journal, 661, 1218, arXiv:astro-ph/0702749

Seager, S., & Hui, L. 2002, Astrophysical Journal, 574, 1004, arXiv:astro-ph/0204225

Sing, D. K., & López-Morales, M. 2009, Astronomy and Astrophysics, 493, L31, 0901.1876

Soffel, M. H. 1989, Relativity in Astrometry, Celestial Mechanics and Geodesy (Relativity in Astrometry, Celestial Mechanics and Geodesy, XIV, 208 pp. 32 figs.. Springer-Verlag Berlin Heidelberg New York. Also Astronomy and Astrophysics Library)

Sotin, C., Grasset, O., & Mocquet, A. 2007, Icarus, 191, 337

Southworth, J. 2008, 0802.3764

Sozzetti, A. et al. 2009, Astrophysical Journal, 691, 1145, 0809.4589

Sterne, T. E. 1939a, Monthly Notices of the RAS, 99, 451

——. 1939b, Monthly Notices of the RAS, 99, 662

Swain, M. R., Vasisht, G., & Tinetti, G. 2008, Nature, 452, 329

Thommes, E. W., Bryden, G., Wu, Y., & Rasio, F. A. 2008, Astrophysical Journal, 675, 1538, arXiv:0706.1235

Torres, G., Winn, J. N., & Holman, M. J. 2008, 0801.1841

Winn, J. N., & Holman, M. J. 2005, Astrophysical Journal, Letters, 628, L159, arXiv:astro-ph/0506468

Winn, J. N. et al. 2007, Astronomical Journal, 134, 1707, arXiv:0707.1908

Winn, J. N., Holman, M. J., Carter, J. A., Torres, G., Osip, D. J., & Beatty, T. 2009a, Astronomical Journal, 137, 3826, 0901.4346

Winn, J. N., Holman, M. J., Shporer, A., Fernández, J., Mazeh, T., Latham, D. W., Charbonneau, D., & Everett, M. E. 2008, Astronomical Journal, 136, 267, arXiv:0804.2479

Winn, J. N. et al. 2009b, ArXiv e-prints, 0902.3461

——. 2006, Astrophysical Journal, Letters, 653, L69, arXiv:astro-ph/0609506

——. 2005, Astrophysical Journal, 631, 1215, arXiv:astro-ph/0504555

Wu, Y., & Goldreich, P. 2002, Astrophysical Journal, 564, 1024, arXiv:astro-ph/0108499

Zharkov, V. N., & Trubitsyn, V. P. 1978, Physics of planetary interiors (Astronomy and Astrophysics Series, Tucson: Pachart, 1978)